



**Politecnico
di Torino**

1-D Morphodynamic simulation of Trebbia riverbed after San Salvatore dam removal

Politecnico di Torino

Master's degree in civil engineering

Academic year 2023/2024

Master thesis

Supervisors:

- Professor Carlo Vincenzo Camporeale
- Doctor Luca Salerno

Student:

- Juan Sebastian Rodriguez Spell S301315

Acknowledgement

This thesis would not have been possible without the emotional support of my fiancée who is the one who gave me the strength to pass through this academic journey. Furthermore, I would like to thank my family for always encouraging me to pursue my dreams, especially because studying overseas without being with them was a tough challenge. Finally, I would like to thank Professor Camporeale and Professor Salerno for all their patience and supportive attitude since the very first time I met them.

Contents

1	Abstract	1
2	Introduction	2
3	Case of study	4
3.1	Dam removal context	6
4	Theoretical framework	7
4.1	Sediment transport in rivers	8
4.2	Indirect methods for the calculation of the total sediment transport	9
4.2.1	H. A. Einstein (1950)	9
4.3	Direct methods for the calculation of the total sediment transport	11
4.3.1	F. Engelund and E. Hansen (1967)	11
4.3.2	Graf and Acaroglu (1968)	11
4.3.3	Ackers and White (1973 and 1993)	12
4.3.4	C. T. Yang 1972	12
4.3.5	Karim 1998	13
4.3.6	S. Yang 2005	13
4.3.7	Contemporary approaches	14
4.4	The non-linear parabolic method	15
4.5	1-D Morphodynamics	16
5	Hydrological analysis	18
5.1	Time series and monthly regime of runoff	19
5.2	Characteristics of the sub-basin	22
5.3	Time of concentration	24
5.4	Probability distribution fitting	25
5.5	Statistical tests	28
5.6	Return period analysis	30
6	Morphodynamic simulation	32
6.1	Grain size distribution	33
6.2	Hydrology	37
6.3	Digital terrain model	38
6.4	Inputs for the simulation	41
7	Results	42
7.1	Evolution of the mean profile	43
7.2	Volume of the pool	46
7.3	Volume transported downstream the dam	48
8	Conclusion	52
9	Annex 1: River's topography	56
10	Annex 2: Main code	60
11	Annex 3: Results processing code	67

List of Figures

1	General location of Trebbia basin within Po basin	4
2	Aerial view of San Salvatore dam	5
3	Time series of daily discharge	19
4	Monthly regime of flow rate from 2005-2023	20
5	Flow duration curve of Trebbia river	21
6	Location of the gauge station	22
7	Time series of hourly discharge	25
8	Annual maxima of discharge	26
9	Histogram of the data and pdf's	27
10	Distributions passing the tests	28
11	Distributions passing the tests	30
12	Variations of return period values	31
13	Location of the photo samples	33
14	Photo 200201	34
15	GSD of photo 200201	34
16	Photo 400401	34
17	GSD of photo 400401	34
18	Photo 900903	34
19	GSD of photo 900903	34
20	Photo 800802	35
21	GSD of photo 800802	35
22	Photo 900901	35
23	GSD of photo 900901	35
24	Photo 900906	35
25	GSD of photo 900906	35
26	Photo 900912	36
27	GSD of photo 900912	36
28	Cloud of points (500 m downstream the dam)	38
29	Segmentation of the cloud	38
30	Digital terrain model for the reach of interest (3km)	39
31	Mean profile of the reach of study	40
32	Migration of the profile for the different time series windows	43
33	Estimated profile after 5 years	44
34	Migration of the profile for the different time series windows	44
35	Estimated profile after 10 years	45
36	3D view of the pool survey	47
37	Volume curve of the pool	47
38	Time series of volume of transported sediments	48
39	Accumulated volume within a five years window	49
40	Time series of volume of transported sediments	50
41	Accumulated volume within a ten years window	50
42	Change of river's bed elevation throughout the years	52
43	3D-view of the evolution of the bed after five years	53
44	Change of river's bed elevation throughout the years	53
45	3D-view of the evolution of the bed after ten years	54
46	200 years return period flood mapping in the nearby of Bobbio town	55

List of Tables

1	Time of concentration by different empirical formulas	24
2	Parameters of the passing distributions	28
3	Discharge for different return periods	31
4	River's topography for the simulation	56

1 Abstract

Dams are recently being demolished for river restoration purposes in order to increase quality and health of the rivers. One of the cases to put into consideration would be San Salvatore dam located in Emilia-Romagna region (Italy) which nowadays is a dam not used for its main purpose but for touristic attraction. This study was conducted to perform a one dimensional assessment of the evolution of the riverbed in the case of the removal of San Salvatore dam. The results shown that the river would recover its natural slope within a period of four years. In contrast, the volume of sediments transported by the removal would not be significant to put in risk of flood the downstream populations.

Le dighe sono state recentemente demolite per scopi di ripristino fluviale al fine di aumentare la qualità e la salute dei fiumi. Uno dei casi da prendere in considerazione sarebbe la diga di San Salvatore situata nella regione Emilia-Romagna (Italia) che oggi è una diga non utilizzata per il suo scopo principale ma per l'attrazione turistica. Questo studio è stato condotto per effettuare una valutazione unidimensionale dell'evoluzione dell'alveo del fiume nel caso della rimozione della diga del San Salvatore. I risultati hanno mostrato che il fiume potrebbe recuperare autonomamente la sua pendenza naturale in un periodo di quattro anni. Al contrario, il volume dei sedimenti trasportati dalla rimozione non sarebbero significativi da mettere a rischio di inondazione le popolazioni a valle.

2 Introduction

Rivers are a source of surface water that have served for millennia to provide the vital resource that human beings and species require for life.

Understanding the interaction of the rivers with the environment that surrounds them, is of vital importance to be able to get an idea of its behavior and also to be able to predict the mechanisms of conservation and its restoration.

Why restoration? because humans have been degrading rivers since we moved from being nomads to creating the first settlement. From this very beginning, rivers have been a source of raw materials for the construction of our settlements, food, waste dumps, and, of course, water to satisfy all of our needs.

To satisfy this last mentioned need, the demand for water, humans have developed infrastructure such as dams to accumulate water to make it available even in dry periods. This type of infrastructure creates a disconnection in the corpse of the river, which triggers environmental impacts such as stopping the migration of fish for their reproduction, cutting the transport of sediments carrying nutrients needed for life of organisms located downstream, and in general, changing the habitat for the species upstream and downstream of the dam.

One example of this is the San Salvatore dam located in the region of Emilia-Romagna, Italy, which was originally built in the twenties in order to satisfy the demand for water for agricultural purposes of the towns surrounding this infrastructure. The construction of the dam was not concluded in its entirety and had an attempt to demolish it, which damaged its top part.

Starting from this context, in terms of river restoration, it would be expected that the removal of the dam will have a positive impact due to the fact that rivers have the ability to heal themselves [23]. Therefore, the purpose of this thesis is to simulate the change in the Trebbia riverbed when the unfinished dam is demolished. In other words, it is intended to predict the morphological evolution of the topography just after the demolition of the dam.

To do so, the study was divided into three main phases explained below: the hydrology, the digital terrain model and, the 1D morphodynamic simulation. The hydrology of the basin was assessed using statistical tools and field measurement records at the point closest to the dam. The time-series of daily and hourly flow rates will be used, and a return period analysis will be performed. Once the main characteristics of the basin were identified, a recent profile of the terrain was required to determine how the dam affected the topography. This is achieved through a DTM obtained from a drone laser survey. In addition, drone surveys can be used to assess the grain size distribution of a riverbed by means of image processing. Finally, using the historical measurements of discharge, the sediment transport for the reach of interest was simulated by solving a nonlinear partial differential equation using the nonlinear parabolic method.

To achieve these goals, academics have developed theories and empirical relationships to describe the phenomena of sediment transport in rivers that will be applied to obtain a one-dimensional approach accompanied by the temporal evolution of the topography. At the end, from one side is expected to find the period of time for the river to turn back

into its natural profile and, on the other hand, to compute the total amount of sediments flushed just after the removal, thus analyzing a possible increment of the riverbed level that concerns the downstream population in terms of flood risk.

3 Case of study

San Salvatore dam is a concrete gravity dam located in the Trebbia river four kilometers upstream the city of Bobbio in the region of Emilia-Romagna, north of Italy. The Trebbia river is a sub-catchment of Po river basin, placed more precisely in the middle part of the basin (right side in the flow direction) in between the sub-catchments of Nura and Taro in the east side and, Scrivia - Curone - Staffora - Luria - Versa - Coppa in the west side [43].

The river is born in the town of Torriglia which is located in the region of Liguria at 800 m.a.s.l., covers length of 111.81 km passing thorough the towns of Fontanarossa, Gorreto, Bobbio, Travo, Rivergaro, San Nicolò covering a total area of 1071.09 km² and flows into the Po river in the vicinity of the city of Piacenza.

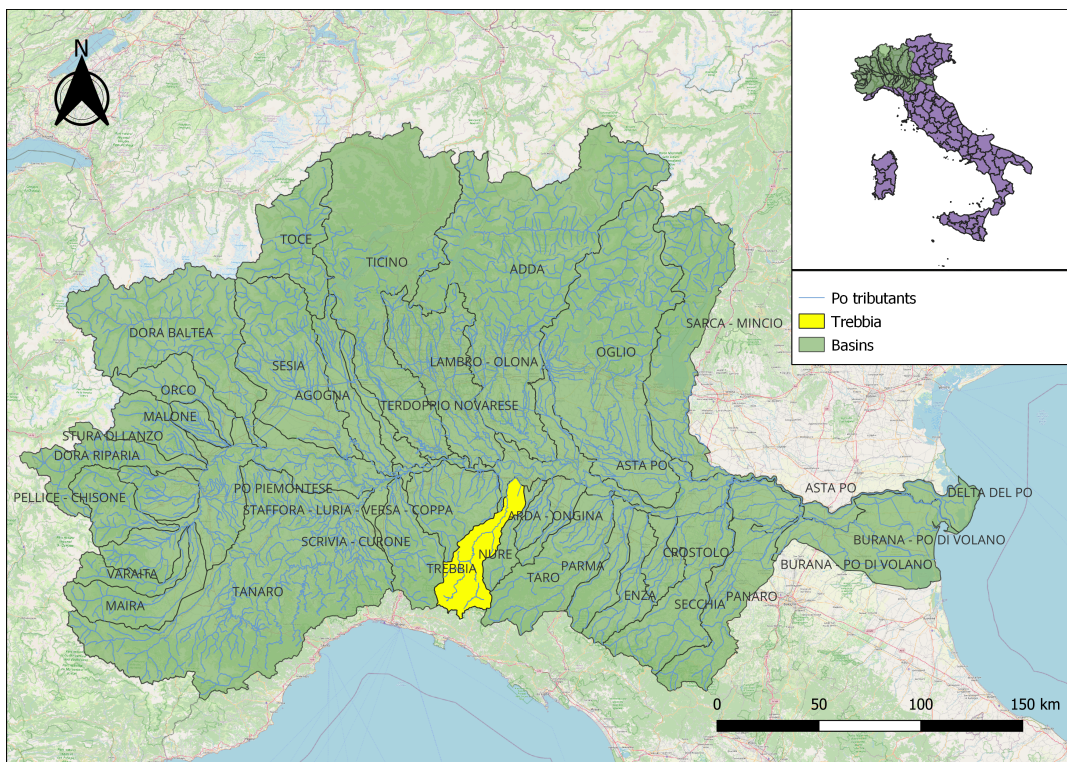


Figure 1: General location of Trebbia basin within Po basin

With respect to the dam, it was originally built for hydropower purposes in charge of the company Terni and its construction started in 1927, then, the project did not see the final milestone due to disputes between the main contractors at the end of 1930 [34]. For the construction, it was implemented a by-pass excavated in the mountains so that the dam's foundation could have been built as well as its superstructure. Nowadays, the by-pass located in the left bank stills being the most used path for the water to travel and has also recreational use for kayakers.

On July 5th 1977, the local kayak club tried to blow up the dam by means of dynamite. Money was collected by the club to afford the "demolition" and few days before they were catching the fishes to put them safe but, the wave of the explosion kill hundreds of them anyways. As a result of this, the dam was damaged by the explosives leaving a rupture on

the top of the weir of the dam [13]. In 2012 was proposed an initiative of a project to build an hydropower plant taking advantage of the already existing infrastructure (the dam and the bypass gallery), both for energy purposes and agriculture, but the idea remained only in the paper due to the though opposition of syndicates and environmentalists [35].

Throughout the years sediments have been depositing upstream the dam almost reaching the top of it and covering with boulders the length between dam and the entrance of the by pass. In contrast, scouring has been occurring downstream the dam lowering the bed of the river day by day and, creating a pool with a central bar. Nowadays the dam is not still used for its initial purposes but, the landscape formed by beaches upstream and the clear waters, are the perfect attraction for tourists in summer season. Besides, the pool is employed to perform diving and the gallery acts as a tunnel for kayakers.



Figure 2: Aerial view of San Salvatore dam

At the end of year 2021 it was officially presented the European program "Open Rivers", which sponsors local associations and organizations willing to restore rivers. This is the case of the "Italian Center of River Re-qualification" (CIRF) which collaborated in the construction of the European program itself, and its working nowadays in the studies of the feasibility of the removal of San Salvatore dam [13]. Lastly, one of the concerns of the inhabitants of Bobbio is regarding the environmental impacts that a civil work of such proportions entails [1].

3.1 Dam removal context

According to the Italian Center for the Rivers Re-qualification (CIRF), there is no register of dam removal performed in Italy leaving the country in the last positions in the ranking performing these kind of efforts regarding river restoration within Europe [38].

The closest reference regarding the "trend" of dam removals is found looking inside Europe, where seventeen countries have reported demolished at least one barrier on their rivers. According to the report of year 2021, the World Fish Migration Foundation (WFMF), a total of 239 dams were removed in Europe, where Spain is the country leading in this aspect having demolished 108 barriers, followed by Sweden with 40 and France with 39, the list is closed by Slovakia accounting for 1 barrier removed [22]. In this perspective, the amount of reaches reconnected within Europe has doubled its quantity comparing with year 2020 where the total number of removed barriers was 101 [41]. Although the numbers previously mentioned seems to be low in comparison to the 1.2 million dams built in European territory, or even against to the 68% of them which corresponds to dams with height not larger than 2 meters [6], it's a promising start and shows that the countries are committed to the recovery of their rivers.

Regarding global trends, according to Ding L. et al (2018) a total of 3869 dams were removed between 1952 to 2016 where the US is the country accounting for the most and, the trend of demolition of dams sharply increased from 1990 to 2010 in Europe and the US and also was expanded to South Asia [15]. Bellmore R. et. al (2017) found that in the US have been removed around 1200 dams by that time, in which unfortunately, less than the 10% of them have pre-damming monitoring and less than four years length post-damming studies [7].

Up to this moment it was only mentioned that dams impose negative consequences to the environment but it's worth to mention what are the impacts of a dam removal. Different efforts have been made in order to measure the consequences or impacts as results of dam removals. For example, in the economical aspect, Lewis L, Bohlen C. and Wilson S. (2008) have found in the US that after a dam removal there is a trend of impacting negatively the real state costs of the properties in the vicinity to the rivers, but the "devaluation" does not persist shortly in time. [33]. Others like Tormos nad van Looy (2014) measured the influence of dams to the macroinvertebrates and fishes finding that, for the macroinvertebrates are sensible for upstream damming density (basin scale) while the fishes are more sensitive to local damming [29]. With respect to rivers morphology, East A. E. (2018) reported that the strongest changes in Elwha river (Washington, USA) morphology occurred within 1-2 years after a dam removal, making the river braided and wider [17] whereas Wilcox C. et al (2014) reported the effects in term of sediment transport for an "instantaneous" dam removal in White Salmon river (Washington, US) where the sudden breach led to 10% of the volume of the impounded sediments to be flushed after two hours of the breach and the 32% of them within days, just comparable to a landslide or an eruption [46].

Inevitably, dam removal should be analysed in the whole spectrum, that is to say, taking into account topics such as: hydraulics, morphology, sediment transport, ecology, habitat, social-economic, politic, engineering but within the scope of this study will be dealt with the one dimensional morphodynamics.

4 Theoretical framework

Demolition of dams is becoming popular for river restoration purposes for those ones that are in disuse or represent any kind of danger [17]. As mentioned before, dams impose a disconnection on the rivers leading to environmental impacts, that is why, removing a dam becomes of paramount importance for river restoration which is the concern of the European water framework directive, the European floods directive and the European habitats directive [45].

From another perspective, big dams are still used for hydropower and storage purposes, therefore, there is another historical fact that intended dam removals are not frequent and field research are only available for relatively small dams ($h < 10m$), which limits the availability of post-removal information [17].

After a dam removal, is expected that the bump of sediments deposited upstream the dam will get flushed, therefore, in order to simulate the evolution in time of the rivers bed after the intended demolition of the dam, is needed to introduce the processes and theoretical background of sediment transport in rivers. This flux (or pulse according to some authors), are field of study of sediment mechanics, topic of interest of geologists, civil and environmental engineers or similar sciences.

On the other hand, as this study will be focus on the one dimensional evolution in time of rivers profile, it was chosen the non- linear parabolic method to describe this phenomena. This choice in particular was made because it is a simple and fast approach (in terms of computational time), suitable for the feasibility stage of this study.

4.1 Sediment transport in rivers

Sediment transport has been studied since nineteenth century specially for navigation purposes. It is commonly agreed that, historically the first approach to determine the bed load of a river is given to Paul du Boys in 1879, where he proposed an expression based on the shear stress on the bed and the critical shear stress to start the movement [26].

$$q_b = \chi \tau_0 (\tau_0 - \tau_{0c}) \quad (1)$$

Eq. 1 is known as the general sediment transport formula and later researchers have done improvements to the formula, based on the concepts of the excess of bed shear stress [14]. These kind of equations receive the name of Du Boys type equations. In 1936 Shields studied the factors influencing sediment transport based on excess of shear stress. Already in twentieth century, Meyer-Peter and Muller (1948) described a new expression including the stream power concept and including the effects of particle roughness [14].

$$\Phi_b = \Gamma (\tau_* - \tau_{*c})^a \quad (2)$$

with $\Gamma = 8$ and $a = 3/2$ for Meyer-Peter and Muller's approach.

H. A. Einstein described the sediment transport as a probabilistic process in 1950 [4]. In year 1956 Bagnold formulated one approach to obtain the bed-load-material through the sum of the bed-load and suspension formulas based on energy concepts. Yalin in 1963 and 1972 introduced a formula starting from probabilistic and energy concepts. Engelund and Hansen developed an empirical formula for the total sediment transport based on energy concepts. Later in 1968 Graf and Acaroglu proposed a formula for open channels and closed conduits based on the shear stress. In 1993 Ackers updated the formula proposed in 1973 with White by correcting the transport rate formula for fine and coarse material. In 1982, Parker proposed a formula to compute the bedload transport for gravel rivers by means of the concept of equal mobility. In 1996 Yang proposed a formula based in energy concepts using a unit stream power formula for sediment-laden flows [26].

Sediment transport has been analysed by many researchers throughout the history and the idea of this text was not to cover all possible theories or experiments developed in history but to give an overview of how long has been studied by academics. Instead of this, the main objective is to revise what of the approaches is suitable for the case of study having in mind that this is a preliminary (feasibility) study of the possible removal. In this sense, as the idea is to predict the evolution of the terrain by the pass of time, is needed to consider both the bedload sediment transport as well as the suspended particles moved along the profile, therefore, next is going to be described some of the approaches accounting for the computation of the total sediment transport.

The total sediment transport or simply called bed-material load by the researches in that field, can be determined by two methods, one indirect approach by calculating the bedload and the suspended load in a separate way to sum up both terms at the end. The direct method corresponds to semi-empirical approach correlating theoretical based formulas with laboratory and field data [14].

4.2 Indirect methods for the calculation of the total sediment transport

Bagnold in 1966 developed two expressions, one based on the energy balance concept for the calculation of the bedload and, one by equating the work done per unit time for sediment suspension to the net stream power for the suspended load. Another approach described by Chang et al 1965 and 1967, calculate the total sediment transport as the sum of the bedload and suspended load based on a Du Boys type expression with a constant K influenced by: the mean velocity, the shear velocity, the sediment size, the shields stress and the slope. [14].

4.2.1 H. A. Einstein (1950)

Hans Albert Einstein worked in a probabilistic theory of sediment transport in 1942 and 1950. In his theory, within the saltation layer the particles are in movement until n number random times then, they stop.

He found out that the average length step is proportional to the mean particle diameter λD where λ tends to 100 [21]. As it is a probabilistic model, the overall jump formula he developed involves the probability of exceeding the submerged weight by the lifting force and the probability that the particle stops after n steps[9]. The overall jump of Einstein approach is described then by:

$$L = \sum_{n=0}^{\infty} (1-p)p^n (n+1)\lambda D = \frac{\lambda D}{1-p} \quad (3)$$

where: L : is length of the overall jump.

n : is the number of steps before the particle stops.

p : is the probability of the lift force exceeding the submerged weight.

λ : Einsteins coefficient tending to 100.

D : The mean diameter of the grain size distribution.

Then, he made the hypothesis that the distribution of velocity at depth $z = 0.35D_c$ is a Gaussian distribution due to turbulence phenomena, where D_c is the characteristic diameter of the grain size distribution. In this way, the probability for motion can be written as:

$$p = 1 - \frac{1}{\sqrt{\pi}} \int_{-\frac{\Psi}{7}-2}^{\frac{\Psi}{7}-2} e^{-t^2} dt \quad (4)$$

and the sediment transport parameter reads:

$$\Phi = \frac{1}{43.5} \frac{p}{1-p} \quad (5)$$

where:

t is only a variable of integration.

Ψ is a parameter that depends on a roughness correction factor, a lifting correction factor and a hiding correction factor $\Psi = f(\chi_k, \zeta, Y)$; based on the dimensionless relationships of $\chi_k = f(D_{65}u'_*/11.6\nu)$, $\zeta = f(D/D_c)$ and $Y = f(D_{65}u'_*/11.6\nu)$ respectively.

On the other hand, for the calculation of the suspended load, Einstein's expression reads:

$$q_s = 11.6u_*C_a a \left[2.303 \log \left(\frac{30.2d}{\Delta} \right) I_1 + I_2 \right] \quad (6)$$

where:

a : is the reference elevation at which a value of concentration is known.

C_a : is the reference concentration at elevation a from the bed.

u_* : is the shear velocity.

d : is the water depth.

Δ : is the submerged relative density.

I_1 and I_2 are the so called Einstein's integrals that can be solved numerically or by the procedure proposed by Einstein himself in 1950. Consequently the total sediment transport is composed by the sum of the bedload transport and the suspended load transport component [18].

Einstein's theory is the most physically based in comparison to the rest of approaches in sediment mechanics. It provides values of dimensionless sediment transport even for values lower than the critical shield stress [9].

4.3 Direct methods for the calculation of the total sediment transport

Again the purpose of this work is not to perform a complete state of art as similar to the efforts of Dey [14] or Gray and Simões [26] or Ancey [4], but to show the most common approaches to compute directly the total sediment transport.

4.3.1 F. Engelund and E. Hansen (1967)

In 1967 Engelund and Hansen performed a collection of the bibliography regarding sediment transport explained in an very practical, educational and engineering perspective, to develop a simple approach to predict the sediment transport based on the similarity principle.

Their work applies for the condition in which the viscous shear is negligible, that is to say for upper flow regime. Then, the dimensionless transport rate is a function of parameters such as friction term and the dimensionless shear stress derived by geometric and dynamic similarities, based on the ratio between the mean depth and the mean diameter of the grain D/d , the slope I , and the effective shield stress θ' [21].

$$f\Phi = 0.1\theta^{5/2} \quad (7)$$

where:

f : is the friction term

Φ : is the non-dimensional transport rate

θ : is the dimensionless shear of the bed or shield stress.

4.3.2 Graf and Acaroglu (1968)

In 1968, Graf and Acaroglu formulated an approach on the basis of about 800 laboratory experiments and 80 field measurements [44]. The assumptions for their work are that, the liquid flow is turbulent, the particles have no cohesion and are uniform in size distributions and finally, saltation and suspended are the main transport mechanisms. It was introduced the concept of "shear intensity" starting from the previous definition of Einstein (1942, 1950), term which was considered only for free surface flows [25].

$$\Phi = 10.39\Psi^{-2.55} \quad (8)$$

where:

Φ : is the transport parameter.

Ψ : is the shear intensity parameter.

4.3.3 Ackers and White (1973 and 1993)

In 1973 Ackers and White derived an expression for the computation of the total sediment load. It was based on physical considerations and dimensional analysis. The authors introduced a dimensionless grain diameter, which expresses the relation between submerged weight and viscous forces (D_{gr}) [44]. Then, the resulting expression for the total sediment transport is:

$$G_{gr} = c \left(\frac{F_{gr}}{A} - 1 \right)^m \quad (9)$$

with the mobility parameter F_{gr} equal to:

$$F_{gr} = \frac{u_*^n}{\sqrt{(s-1)gd}} \left(\frac{U}{\sqrt{32 \log\left(\frac{10Y}{d}\right)}} \right)^{1-n} \quad (10)$$

where:

G_{gr} : is the transport parameter

u_* : is the shear velocity [m/s]

s : is the specific gravity of the sediment

g : is the gravitation acceleration [m/s²]

d : is the grain diameter [mm]

U : is the mean velocity in the river [m/s]

Y : is the water depth [m]

n , m , A , c are parameters calibrated from 1250 field and laboratory experiments. The values of these parameters are constant for a $D_{gr} > 60$ and corresponds to 0, 1.78, 0.17, 0.025.

4.3.4 C. T. Yang 1972

According to Yang, previous formulae for the computation of the total sediment transport presented difficulties thanks to the unrealistic assumptions previously done, therefore, it has been introduced the term of "unit stream power" [47]. By means of a multiple regression analysis he obtained the following relation for the logarithm of the total sediment concentration:

$$\begin{aligned} \text{Log}C_t = & 5.435 - 0.286 \log\left(\frac{\omega d}{\nu}\right) - 0.457 \log\left(\frac{U_*}{\omega}\right) \\ & + \left[1.799 - 0.409 \log\left(\frac{\omega d}{\nu}\right) - 0.314 \log\left(\frac{U_*}{\omega}\right) \right] \log\left(\frac{VS - V_{cr}S}{\omega}\right) \end{aligned} \quad (11)$$

where:

d : is the particle size.

ω : is the fall velocity.

U_* : is the shear velocity.

ν : is the kinematic viscosity.

$\left(\frac{VS-V_{cr}S}{\omega}\right)$: is the dimensionless unit stream power.

4.3.5 Karim 1998

Using the same experimental and field data from Karim and Kennedy 1990, Karim derived a simpler empirical expression to determine the total sediment transport including the resistance of bedforms [30]. The expression reads [14]:

$$\Phi_t = 1.39x10^{-3} F_d^{2.97} \left(\frac{u_*}{w_s}\right)^{1.47} \quad (12)$$

where:

F_d : is the resistance due to the bedforms

u_* : is the shear velocity

w_s : is the terminal fall velocity of the particle

4.3.6 S. Yang 2005

In 2005, Yang proposed a new formula for the computation of the total sediment load by means of 3500 data sets analyzed. The total sediment transport depends on a new defined transport parameter and a coefficient of proportionality. The new transport parameter includes a combination of variables such as: water depth, hydraulic radius, mean velocity, energy slope, shear stress and sediment size; variables that other researchers had not taken into account before all together. Moreover, this new parameter achieve a coefficient of correlation of 0.987 [48]. The expression of Yang is the following:

$$g_t = k \left(\frac{\gamma_s}{\gamma_s - \gamma}\right) T_T \quad (13)$$

and the total-load transport parameter T_T :

$$T_T = \frac{\tau_0(u_*'^2 - u_{*c}^2)}{\omega} \quad (14)$$

where:

k : is the coefficient of proportionality that tends to 12.5.

γ : is the specific weight of the water.

γ_s : is the specific weight of the sediment.

τ_0 : is the bed shear stress.

$u_*'^2$: is the shear velocity due to the grain.

u_{*c}^2 : is the Shield's critical shear velocity

ω : is the fall velocity of the particle.

One consideration for Yang's approach, is that the formula was verified mainly on sandy rivers.

4.3.7 Contemporary approaches

In 2012, B. Kumar employed 1200 both field and flume data sets measurements of variables such as: discharge, width, depth, friction factor, mean diameter, shear stress, shield stress, gradation coefficient, specific gravity, viscosity and the Bed form typology; to apply an Artificial Neural Network (ANN) to understand the complex relation of the input and output vectors. As compared to the "classical methods" which drop coefficients of determination R^2 values between 0.65 to 0.78, Kumar reached statistical performances around 95% and 97% between the observed data and predicted data [31].

In recent times, 2023, researchers of the Indian Institute of Technology worked with methods such as: linear regression models, deep neural network, extreme learning machine and support vector regression to predict sediment transport reaching statistical performances of 0.96 coefficient of determination R^2 [42].

4.4 The non-linear parabolic method

Before talking about the non-linear parabolic method it is worth explaining what a partial differential equation is. A partial differential equation is an equation in which the unknowns are function of at least two independent variables and its partial derivatives [32]. One of the most common examples of a partial differential equation is the heat equation (or diffusion equation) in which the change of temperature in time on a time-space domain is equal to a diffusion coefficient times the second derivative in space. The diffusion equation has the following form:

$$\frac{\partial}{\partial t}u(x, t) = \frac{\partial^2}{\partial x^2}u(x, t) \quad (15)$$

where:

u : is the temperature.

x : is the space domain.

t : is the time domain.

Likewise, a linear second-order partial differential equation, commonly named PDE, has the following shape:

$$A \frac{\partial^2 u}{\partial x^2} + B \frac{\partial^2 u}{\partial x \partial y} + C \frac{\partial^2 u}{\partial y^2} + D \frac{\partial u}{\partial x} + E \frac{\partial u}{\partial y} + Fu = G \quad (16)$$

where A , B , C , D , E , F , G can depend on x and y but not on u . In this way, if a second-order partial differential equation has a different form than the previously described equation, it means it is nonlinear [32]. On the other hand, depending on the solution the partial differential equations can be classified as:

- Elliptic if $B^2 - 4AC < 0$
- Hyperbolic if $B^2 - 4AC > 0$
- Parabolic if $B^2 - 4AC = 0$

In this context, changes in rivers bed due to sediment transport processes often are modeled using simplified nonlinear diffusion equations [16]. For example, Cantelli A. and Parker G. et al (2007) derived a 2-D numerical model to study the erosion/accretion in a river caused by a dam removal [11]. However, the focus on this study will consider the 1-D morphodynamics approach also proposed by Parker G. (2004) [24].

4.5 1-D Morphodynamics

The physical phenomena occurring in a river are influenced by the hydrodynamics and morphodynamics. Hydrodynamics for open channels which means the changes in depth and flow, are described using de Saint Venant equations Eq. 17 and Eq. 18, while, the changes in the bed of the river is determined by means of the Exner equation Eq. 19. The details of the formal derivation of these following expressions can be found in Camporeale [10] or Dey [14].

$$\frac{\partial \Omega}{\partial t} + \frac{\partial Q}{\partial x} = 0 \quad (17)$$

$$\frac{\partial Q}{\partial t} + \frac{\partial}{\partial x} \left(\beta \frac{Q^2}{\Omega} \right) + g\Omega \left(\frac{\partial h}{\partial x} + \frac{\partial \eta}{\partial x} \right) + \frac{Q^2}{\Omega C^2 R} = 0 \quad (18)$$

$$(1-p)b_f \frac{\partial \eta}{\partial t} + \frac{\partial}{\partial x} (b_f q_{bx}) = 0 \quad (19)$$

where x and t are the spatial-temporal domain and:

Ω : is the channel cross section.

Q : is the discharge passing through the channel.

β : is the correction factor for the distribution of stresses on the cross section

g : is the gravitational acceleration.

h : is the water depth.

η : is the channel's bed elevation.

C : is the conductance.

R : is the hydraulic radius.

p : is the porosity.

b_f : is the channel's bed width.

q_{bx} : volume of bedload sediment transport.

As the scope of the study deals with 1-D modeling, everything must be written in terms of time and space, that is to say, the independent variables are the time and space and, the dependent variables are the discharge, the bed topography and the cross section of the channel [10].

Thus, combining bedload sediment transport formula Eq. 1 and Chezy equation in terms of the unitary discharge Eq. 20, Parker G. [16] obtained a formula Eq. 21 for the sediment transport to be solved [10]:

$$q = k_s h^{5/3} \sqrt{S} \quad (20)$$

$$q_b = \Gamma \sqrt{\Delta g D^3} (\Omega S^{7/10} - \tau_{*c})^a \quad (21)$$

Then, computing the partial derivative of the previous expression it can be obtained the following second order partial differential equation with ($S = \frac{\partial \eta}{\partial x}$):

$$\frac{\partial q_b}{\partial x} = -\Gamma \sqrt{\Delta g D^3} \left(\frac{7\Omega}{10} \right) \left(-\frac{\partial \eta}{\partial x} \right)^{-3/10} \left(\Omega \left(-\frac{\partial \eta}{\partial x} \right)^{7/10} - \tau_{*c} \right)^{a-1} \frac{\partial^2 \eta}{\partial x^2} \quad (22)$$

where:

k_s : is the roughness Stickle's coefficient.

S : is the slope of the channel.

τ_{*c} : is the critical shields stress.

a : is an exponent which depends on the sediment transport formula to be used.

D : is the grain size diameter.

Γ : is a factor which will depend on the sediment transport formula to be used.

The partial derivative of the sediment transport from Eq. 22 can be replaced in Exner equation Eq. 19, thus obtaining the formula to be resolved by the nonlinear parabolic method:

$$(1 - p) \frac{\partial \eta}{\partial t} = F \frac{\partial^2 \eta}{\partial x^2} \quad (23)$$

where F is equal to $F = -\Gamma \sqrt{\Delta g D^3} \left(\frac{7\Omega}{10}\right) \left(-\frac{\partial \eta}{\partial x}\right)^{-3/10} \left(\Omega \left(-\frac{\partial \eta}{\partial x}\right)^{7/10} - \tau_{*c}\right)^{a-1}$

5 Hydrological analysis

To perform the hydrological analysis, were found two main gauges close to the area of the dam, the first one corresponds to a hydrometer located in the downtown of Marsaglia, a town located 7.42 *km* upstream San Salvatore dam. This hydrometer located at the "Ponte di Marsaglia" bridge, counts with measurements of water depth from the year 2011 up to the present but, there is no information about the rating curve or any calibration for the rule according to the information provided by the Regional Agency for the Environmental Protection (ARPA) of Emilia-Romagna.

The second gauge is an hydrometer situated under San Martino bridge in the town of Bobbio 3 *km* downstream the dam. For this station, there is information of hourly and daily data of flow rate available from year 1997 up to the present. From the same year, ARPA also releases a yearly report of the parameters read by every station of its jurisprudence, including reports of extreme events and annual rating curves for the case of those stations measuring flow rates.

Therefore, because of the proximity, the reliability and completeness of the data, the chosen station to be analyzed will be Bobbio. Location of the gauge station is displayed in Fig. 3.

5.1 Time series and monthly regime of runoff

From the Bobbio gauge station can both be obtained the mean daily and hourly data. There is reliable information (without gaps and revised) from year 2005 up to present [12]. Following is presented the time series of mean daily flow rate:

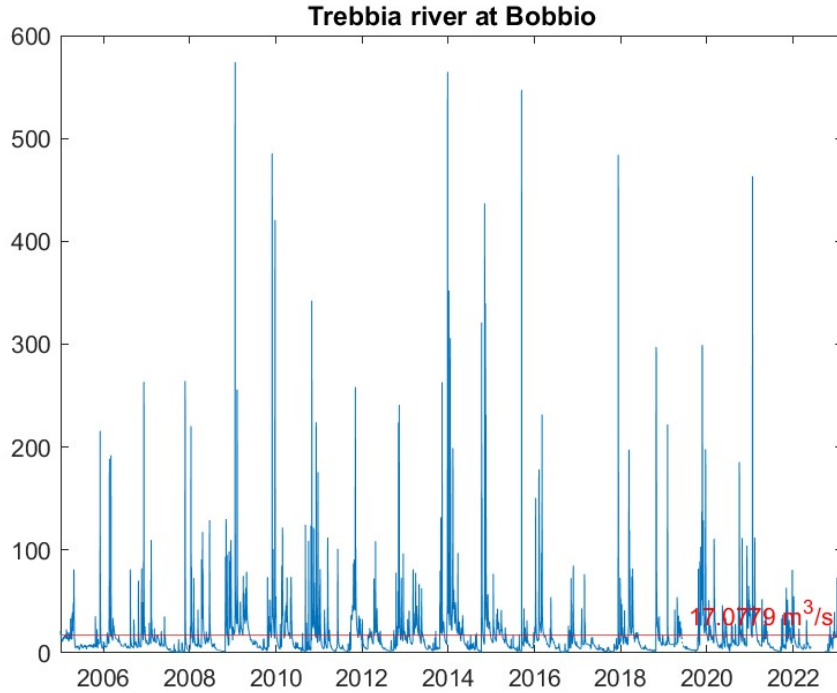


Figure 3: Time series of daily discharge

According to the data, the mean value of flow rate in the river is $Q_{mean} = 17.08 \text{ m}^3/s$, likewise presenting a minimum value of $Q_{min} = 0.36 \text{ m}^3/s$ and a maximum value of $Q_{max} = 574.07 \text{ m}^3/s$. On the other hand, the seasonal behavior of the river within a calendar year can be visualized through the monthly regime displayed in Fig. 4. The river exposes a partially snow affected catchment behavior where, there are high flows during the rainy periods usually present in the spring and autumn and, dry periods in summer. In addition to this, spring high flows are intensified due the melting of the snow over the Apennines.

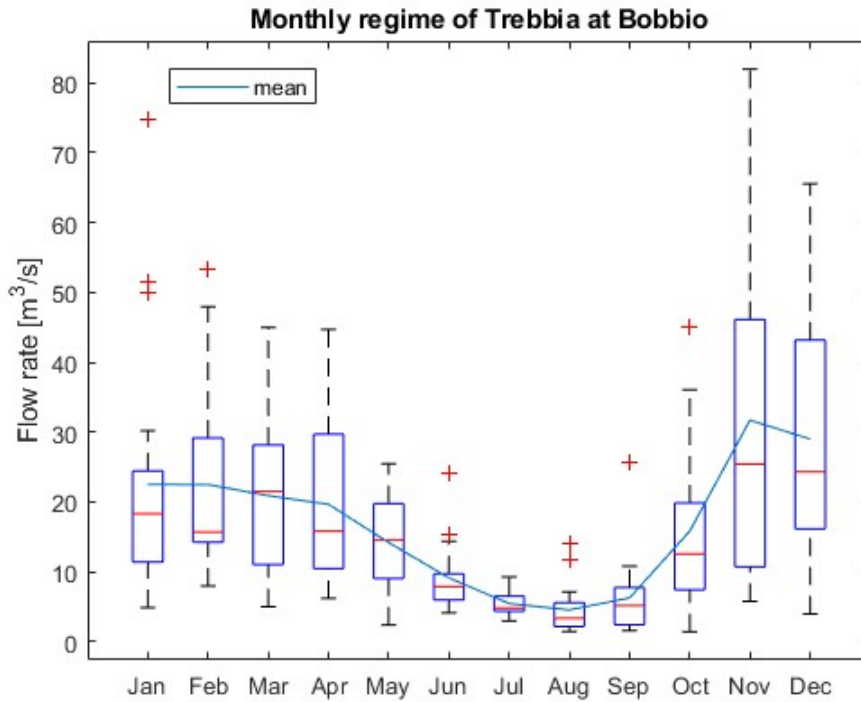


Figure 4: Monthly regime of flow rate from 2005-2023

Statistically speaking in Fig. 4 the red line displays the median, upper blue line displays the 75th percentile, lower blue line displays the 25th percentile, top black line the maximum and bottom black minimum value. Lastly, the red crosses represent the outliers. From the monthly regime of runoff it can be said the amount of water in summer periods is almost certain whereas, end of autumn and spring months are the one accounting for the more uncertainty.

If one classify the information in a calendar year, one can build the flow duration curve for each of the years. The average of them describes the flow duration curve of the river useful to estimate how many days a year can exceed certain value.

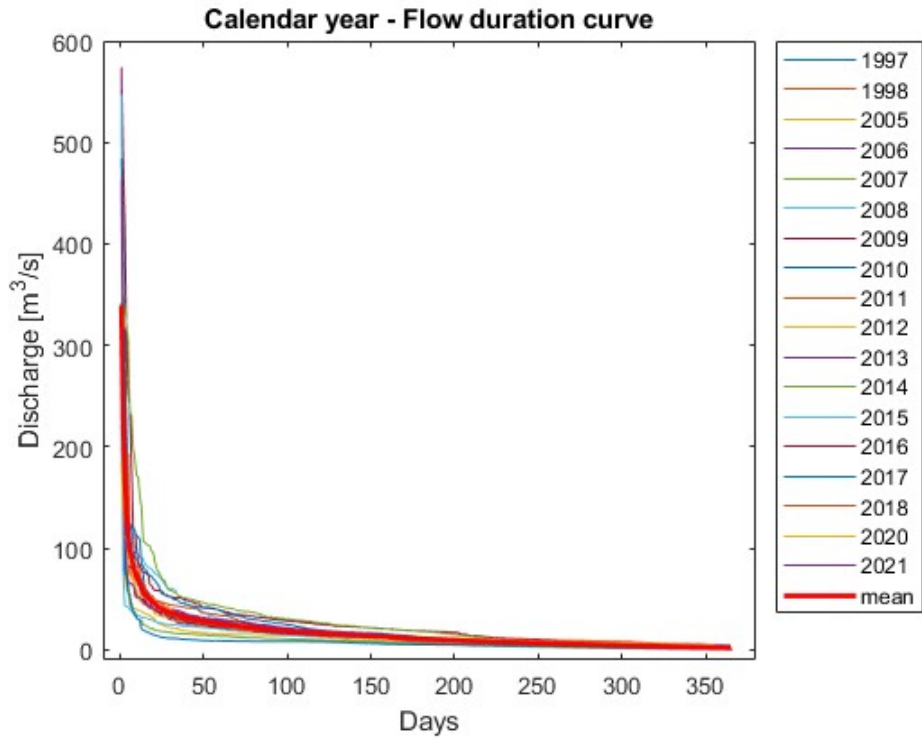


Figure 5: Flow duration curve of Trebbia river

To build the flow duration curves it was used the data of years counting with measurements all days of the year. In Fig. 5, the colored lines represent the FDC for every year of the time series whereas the red line represents the averaged FDC throughout the years. In next table can be observed the amount of days exceeding the corresponding discharge value according to the averaged FDC:

Duration of the discharge	
Days	1997-2021 [m^3/s]
10	72.20
30	36.96
60	25.82
91	19.75
135	14.71
182	10.79
274	5.46
355	2.27

5.2 Characteristics of the sub-basin

The gauge station "Bobbio" is situated in the following coordinates: $9^{\circ}23'1.30$ E, $44^{\circ}45'18.3$ 7 N under the San Martino bridge. Consequently, the created sub-catchment which starts on the source of the river to the gauge, covers an area of 655 km^2 and the distance (in the direction of the flow) from the source of the river to the station is 56.5 km .

On the other hand, from the Digital Elevation Model (DEM) $10 \times 10 \text{ m}$ cell size obtained from the National Institute of Geophysics and Vulcanology (NIGV) [40], was obtained that the maximum elevation of the basin corresponds to $Z_{max} = 1724.77 \text{ m}$, the mean elevation of the basin $Z_{mean} = 942.20 \text{ m}$ and $Z_{min} = 257.53 \text{ m}$ is the elevation at the outlet. The shape of the new basin and the location of the gauge are shown in Fig. 6.

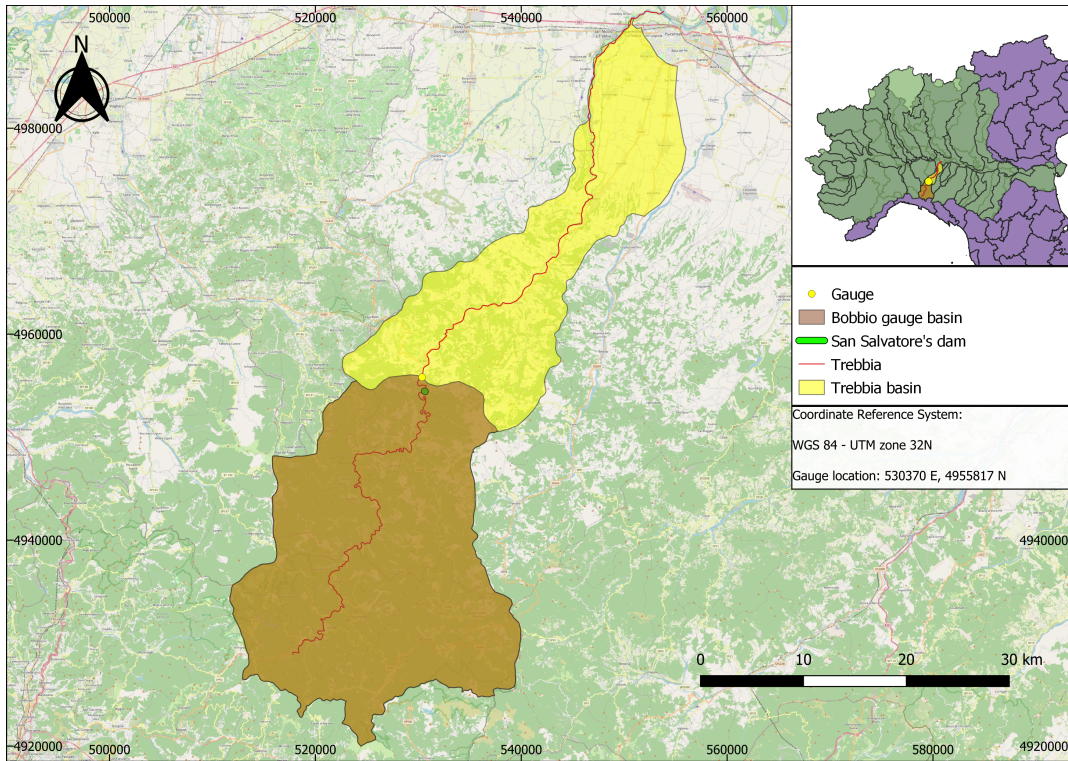


Figure 6: Location of the gauge station

Regarding the topography of the basin, it is mainly characterized by hilly-mountainous although Trebbia river has a mean slope of 7.7% .

Main tributary rivers to the sub-catchment are Boreca creek, Avagnone creek and Aveto river, this last one accounting for a surface of 257 km^2 . The stream section appears constantly recessed, deeply engraved in the rocky substrate, with a morphology characterized by meanders in very irregular rock, with generally high curvature, slowly evolving [36].

In terms of infrastructure influencing the natural discharge of Trebbia, there are not big significant dams upstream affecting the regulation of the river, although there are two dams in the basin that were built for hydropower, irrigation and water supply purposes [27]. The first one is located in the Brugneto creek, tributary to the Trebbia in the west side, but part of the administrative territory of the region of Liguria. The capacity of the reservoir held by Brugneto dam accounts for 24 Mm^3 . The second dam, is a modest

dam situated at the Aveto river, tributant in the east side of Trebbia with a volume of 0.8 Mm^3 [3]. There is a third dam located in Boreca creek [37] with a reservoir with capacity equal to 0.07 Mm^3 [20].

With respect to irrigation channels, they are located in sections downstream the gauge station, which means there are no significant water withdrawals for irrigation purposes within the sub-basin.

Regarding the administrative borders, the sub-basin is immersed within two regions: Emilia-Romagna (48.2%) and Liguria (51.8%) in the most upstream part.

Trebbia is characterized by a notable solid transport capacity, reduced in recent years due to the arrangement of the tributaries. The watercourse in the upper part it has a sunken riverbed, with rocky and elevated banks slope. In the intermediate section the riverbed is made up of poor materials consistency and in the final one it flows in a large conoid that extends up at the mouth of the Po [27].

Morphologically the area belongs to the Piacenza Apennines, characterized in particular from the depth of the valley furrows dug by the watercourses inside of the mountain mass, consisting mainly of clayey shale and only in some areas with serpentines, much less erodible and therefore highly visible connoting the landscape [27].

5.3 Time of concentration

In the hydrological context, one parameter that gives an idea of shape and peak of runoff hydrographs is the time of concentration [28], which can be estimated by empirical formulas like the ones proposed by Giandotti (1934), Kirpich (1940) and Department of Public Works of the United States (1995) [39]. For this purpose Giandotti's formula reads:

$$T_c = \frac{4\sqrt{A} + 1.5L}{0.8\sqrt{H}} \quad (24)$$

where T_c is the time of concentration in hours, A is the area of the catchment in square kilometers, L is the length of the main channel in kilometers and H , the difference between the mean elevation of the catchment and the elevation of the gauge or outlet in meters. On the other hand, Kirpich equation is:

$$T_c = 0.0078L^{0.77}S^{-0.385} \quad (25)$$

where T_c is the time of concentration in minutes, L is the length of the main channel in feet and S , the mean basin slope. Finally, the Department of Public Works formula is the next one:

$$T_c = 60 \left(\frac{11.9L^3}{H} \right)^{0.385} \quad (26)$$

where T_c is the time of concentration in minutes, L is the length of the main channel in miles and H , is the maximum difference in meters between the outlet elevation and any catchment limit elevation. The mentioned three formulas were used because they were conceived and calibrated for small basins (170 to 70,000 km^2)[39]. Applying previous formulas one gets the following results:

Time of concentration of the basin				
Giandotti [h]	Kirpich [h]	DPWUSA [h]	Mean (μ) [h]	Std (σ) [h]
8.94	9.67	18.14	12.25	5.11

Table 1: Time of concentration by different empirical formulas

Averaging the formulas one get that the time of concentration of the basin is $T_c = 12.25 \pm 5.11$ hours.

5.4 Probability distribution fitting

The hydrological data comes from the previous mentioned gauge station managed by ARPA Emilia-Romagna and counts with measurements of hourly flow rate from 1997 to 2023 [19]. The following figure shows the flow rate time series:

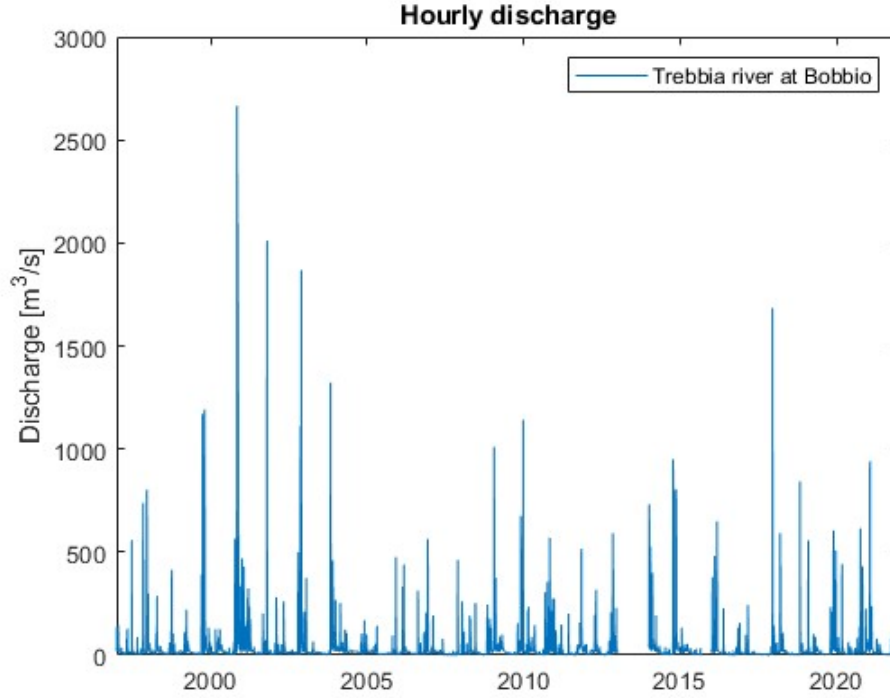


Figure 7: Time series of hourly discharge

From the Fig. 7 it can be observed that in years 2013 and 2015 there is a gap in the time series. Comparing with the annual records reported by ARPA, these gaps are tightly related to extreme events that could have damaged the gauges or exceeded the maximum measurable level. Moreover, it can be seen that there is a defined rainy period every year in the months of October and November corresponding to the peaks of maximum discharge of the graph. According to this data, the mean value of discharge of Trebbia at Bobbio is equal to $Q_{mean} = 19.72m^3/s$.

With the purpose of calculating the values of flow rate corresponding to return periods of flood is needed to find the annual maximum values. Then, extracting the information of the annual maximum value of the time series of Fig. 4, it can be obtained the following graph:

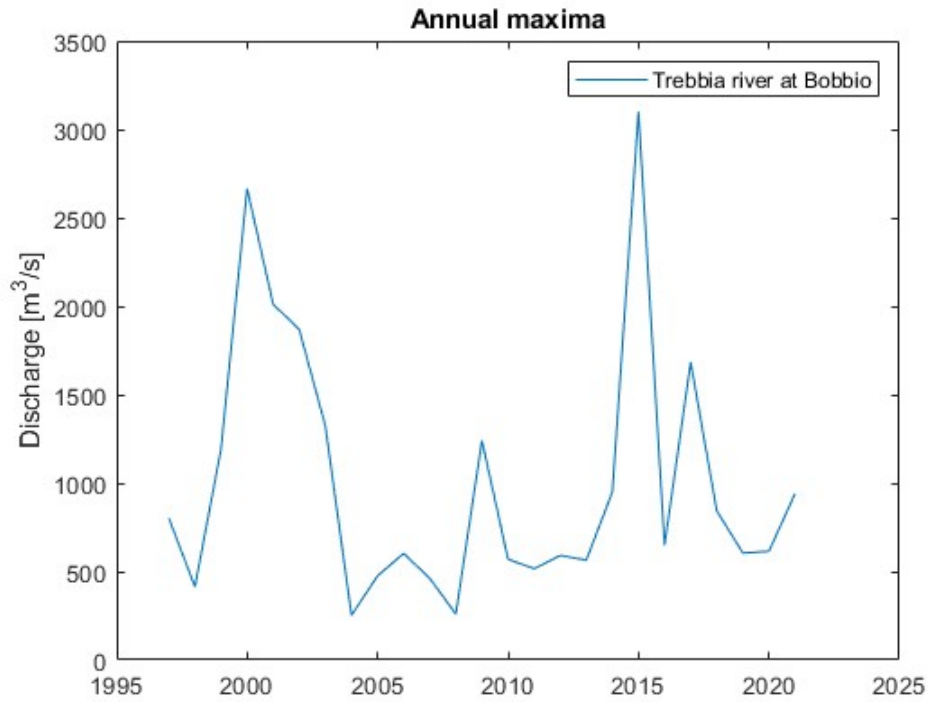


Figure 8: Annual maxima of discharge

Maximum events of year 2006, 2009 and 2015 were reconstructed with the data of annual reports of ARPA Emilia-Romagna [5]. It is interesting to note how variable can be the discharge in the river considering that is almost null in some periods of the time series, but at the same time, exhibiting extreme events such as the one of 2015 accounting for $3100 \text{ m}^3/\text{s}$. Even the mean discharge is two orders of magnitude lower than the maximum event.

Regarding the statistical inference topic, statistical distributions such as: the Normal distribution, Log-normal, Generalized Extreme Value (GEV), Exponential, Gamma, Weibull and Log-Logistic were tested to see which of them fit to the observations. In Fig. 6 are shown the probability density functions of the distributions that better follows the trend of the histogram of the data.

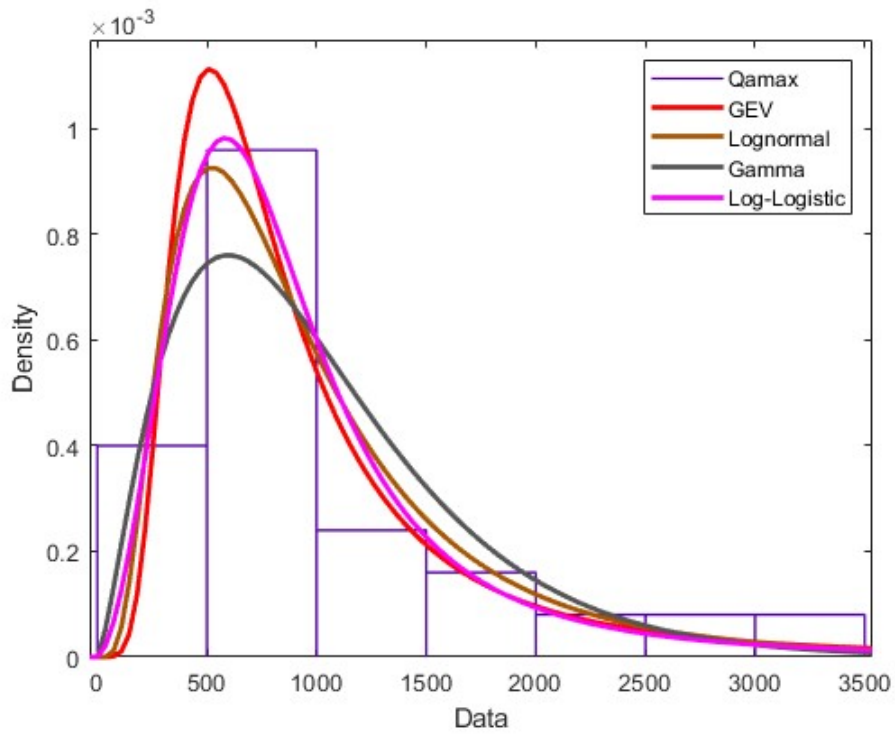


Figure 9: Histogram of the data and pdf's

According to Fig. 6, the histogram of the data is skewed right as normally do the extreme events in hydrological studies. In order to see which distribution to discard or those distributions which fit well to the data, test of goodness of fit are going to be performed in the next subsection.

5.5 Statistical tests

The distributions mentioned in subsection 5.4 have been tested using the Chi-squared, Anderson-Darling and Kolmogorov-Smirnov tests while the estimation of parameters was made using maximum likelihood method.

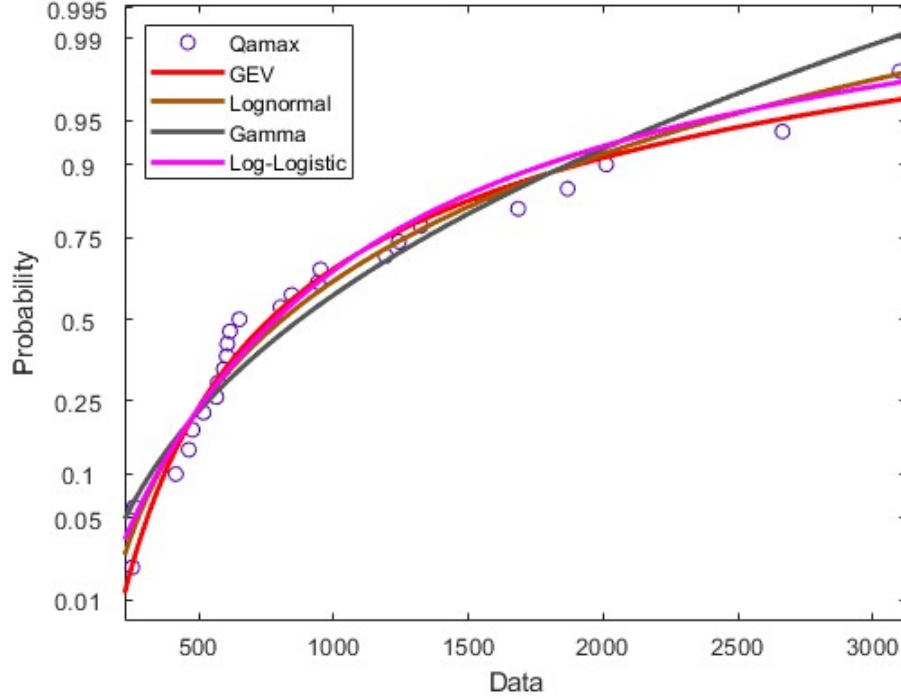


Figure 10: Distributions passing the tests

Probability distributions				
Parameter	Log-logistic	GEV	Log-normal	Gamma
Location [μ]	6.664	622.733	6.698	N/A
Scale [σ]	0.375	354.200	0.660	411.435 ¹
Shape [κ]	N/A	0.396	N/A	2.449 ²

¹ Rate parameter [β]

² Shape parameter [α]

Table 2: Parameters of the passing distributions

At the end of the tests, it was found that four distributions have passed all the tests. Therefore, for the return period analysis GEV, Log-normal, Gamma and Log-logistic were employed. The following equations represent the probability density function for the passing distributions:

1) GEV distribution:

$$p(x) = \frac{1}{354.2} \left(1 - \frac{0.396}{354.2}(x - 622.733)\right)^{\frac{(1-0.396)}{0.396}} \exp\left(-\left(1 - \frac{0.396}{354.2}(x - 622.733)\right)^{\frac{1}{0.396}}\right) \quad (27)$$

2) Log-normal distribution:

$$p(x) = \frac{1}{0.66x\sqrt{2\pi}} \exp\left(-\frac{1}{2} \left(\frac{\ln(x) - 6.698}{0.66}\right)^2\right); x > 0 \quad (28)$$

3) Gamma distribution:

$$p(x) = \frac{411.435}{\Gamma(2.449)} x^{2.449-1} e^{-411.435x} \quad (29)$$

4) Log-logistic distribution:

$$p(x) = \frac{1}{0.375} \frac{1}{x} \frac{e^z}{(1 + e^z)^2}; x \geq 0 \quad (30)$$

where:

$$z = \frac{\log(x) - 6.664}{0.375}$$

5.6 Return period analysis

The return period analysis was performed as one of the concerns of the dam demolition is the fact of transporting a huge amount of sediments downstream the dam, in such a way that, the risk of flood is increased due to the raising of river's bed. In this sense, the values of flow rate for 2, 5, 10, 20, 50, 100, 200 year return periods were calculated for each of the passing distributions. As more than one distribution has passed the tests, the design value was estimated with the mean of the values corresponding to each return period.

In Fig. 11 red circles are marking the values of return period for each year of analysis for the studied distributions while in table 3 are found the corresponding values for each mark. In the quantile plot one can see in red line the GEV distribution, in yellow the log-normal distribution, in purple the Gamma distribution and in cyan the log-logistic distribution. Return periods and probability of exceedance are related with the following expression:

$$p = 1 - \left(1 - \frac{1}{T}\right) \quad (31)$$

where T is the return period in years and p is the probability of exceedance.

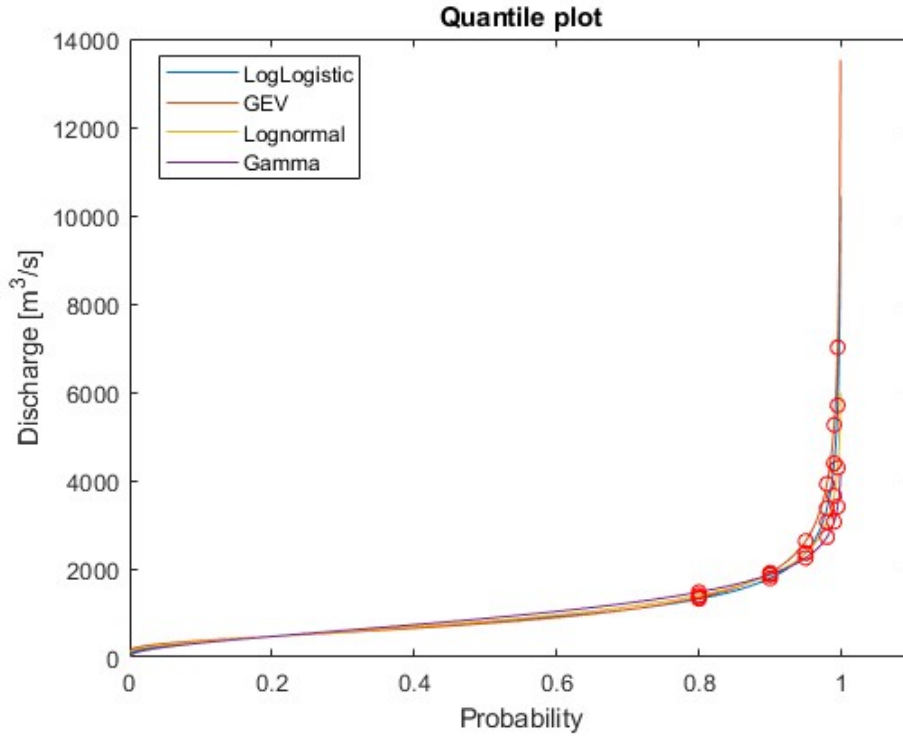


Figure 11: Distributions passing the tests

Return period [years]	Log-logistic [m^3/s]	GEV [m^3/s]	Log-normal [m^3/s]	Gamma [m^3/s]	Mean (μ) [m^3/s]	Std (σ) [m^3/s]	CV [%]
2	783.47	762.45	810.49	874.40	807.70	48.62	6.02
5	1317.54	1348.32	1397.08	1472.73	1383.92	67.66	4.89
10	1785.72	1908.96	1857.07	1870.20	1855.49	51.46	2.77
20	2363.14	2628.29	2349.13	2245.02	2396.40	163.33	6.82
50	3371.01	3922.55	3060.53	2719.09	3268.30	511.01	15.64
100	4388.18	5258.57	3650.82	3066.64	4091.05	947.74	23.17
200	5701.33	7012.82	4290.31	3407.23	5102.92	1585.51	31.07

Table 3: Discharge for different return periods

As seen in table 3, the significant variations are found in large return periods, the rest of them are in an acceptable range. According to this, the mean value corresponding to the 50 years return period is equivalent to the maximum event reported in the time series. In the following figure are visible the graphical representation of the percentiles for the different return periods.

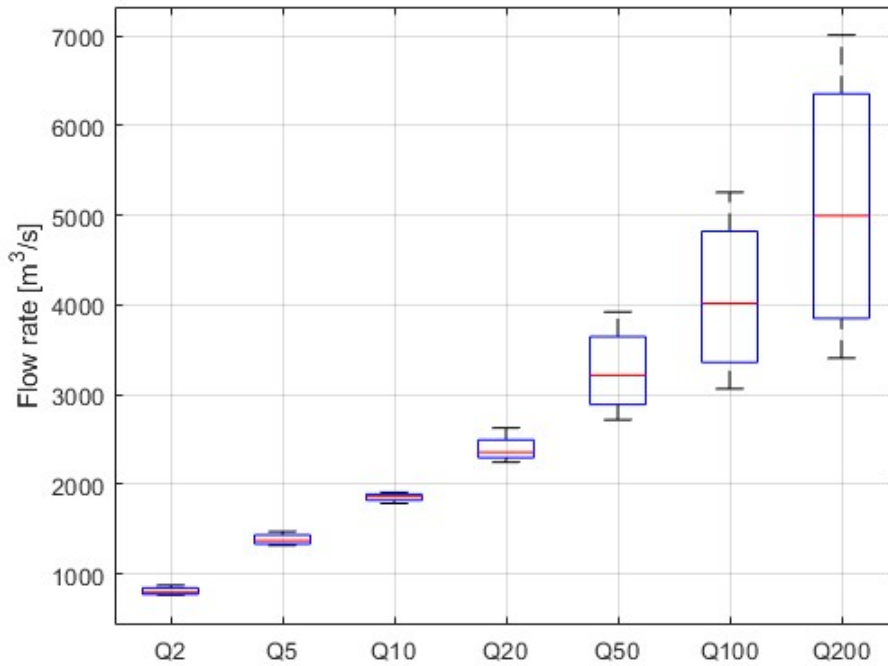


Figure 12: Variations of return period values

Statistically speaking in Fig. 12 the red line displays the median, upper blue line of the box displays the 75th percentile, lower blue line of the box displays the 25th percentile, top black line the maximum and bottom black minimum value. Additionally, climate change may increase the variations and frequencies of extreme events but because of the time scale of the problem, these effects will not be considered.

6 Morphodynamic simulation

In order to perform the morphodynamic simulation, formulas from subsection 4.3 must be used to determine the transport of sediments within the reach of interest. Regarding the previously exposed in subsection 4.3, experimental data has shown that Engelund Hansen approach drops larger values of sediment transport while Einstein procedure gives lower values [17]. On the other hand, Graf and Acaroglu drops mid to low values. According to Simões and Gray [26], Karim's formula 4.3.5 does not work very well for armored beds which is one of the most common conditions found on site in Trebbia's reach of interest. Similarly, same authors exposed that Yang's formula 4.3.4 works better for silt rivers.

Therefore, for the purpose of this study and in order to have a conservative approach it will be considered Engelund-Hansen formula for the simulation of the evolution of the river's bed. By opting for that formula, from one side the computational time and memory are small and, from the other side, for the scope of the study is enough as the objective is not concentrated in exact values of sediment transport but in the morphological evolution of the profile.

Lastly, Engelund and Hansen formula (1967) 4.3.1 is useful because it considers the total sediment transport in direct form, that is to say, including both the bedload sediment transport and suspended bedload sediment transport[8]

Regarding the parabolic method, it has the advantage of including a diffusion term which makes is suitable for the desired application [10], if one compares with the kinematic model where amplitude of sediment waves remain constant in time.

Consequently, the morphodynamic simulation was made by means of the parabolic method and Engelund and Hansen approach. Then, the required inputs for the simulation are explained in the following subsections.

6.1 Grain size distribution

In April 12th 2023, it was performed a drone survey to get photographs of the riparian areas of Trebbia river specially in the closeness to the dam. The photos were taken considering a reach distance of 300 meters upstream the dam and 400 meters for downstream. The objective of the analysis were the dry areas and bars present on the stream as shown in the following figure:

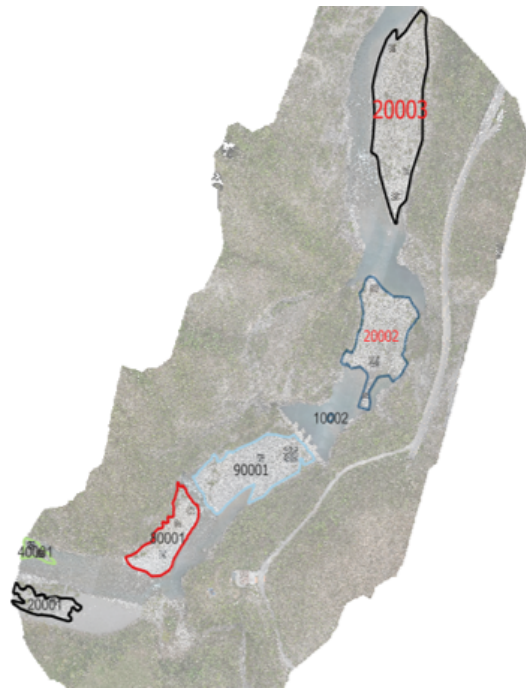


Figure 13: Location of the photo samples

The number given to the areas are the following starting from upstream: 40001, 20001, 80001, 90001, 10002, 20002, 20003. Within each sampled area were taken sub-samples and the grain size distribution of each area consists in the average of the sub-samples. The samples were analysed by imaging processing software to obtain the grain size distribution of each of them, to do so, it was used a size of pixel of 13.9 mm.

At the end, seven photos had enough resolution to perform the analysis hence, the results of grain size distribution are displayed in the following figures:



Figure 14: Photo 200201

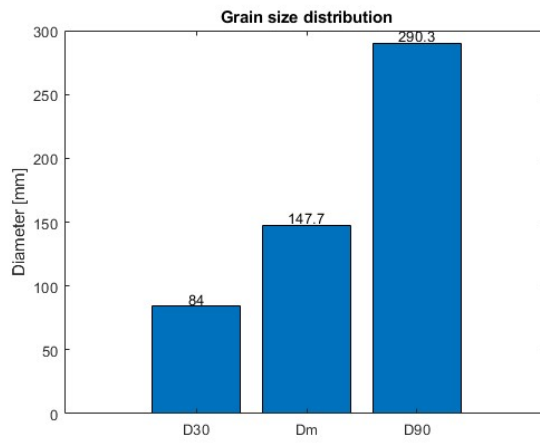


Figure 15: GSD of photo 200201



Figure 16: Photo 400401

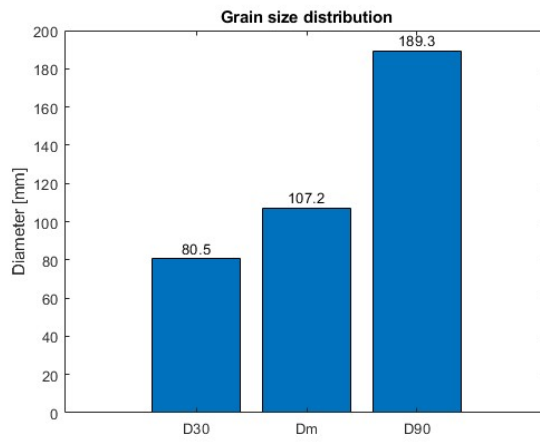


Figure 17: GSD of photo 400401



Figure 18: Photo 900903

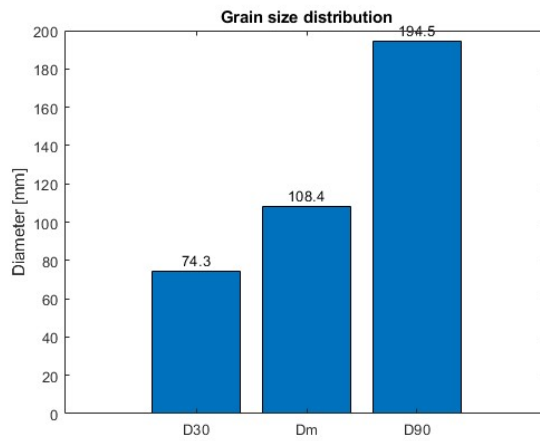


Figure 19: GSD of photo 900903



Figure 20: Photo 800802

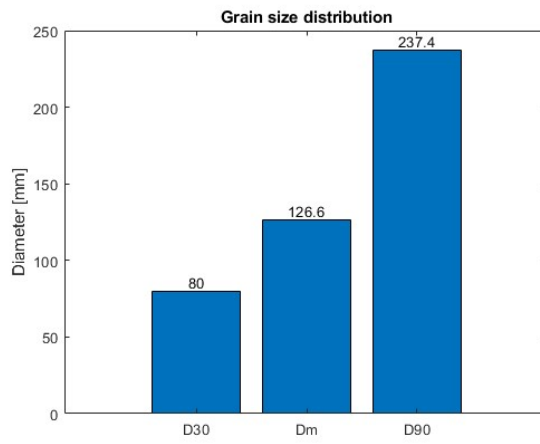


Figure 21: GSD of photo 800802



Figure 22: Photo 900901

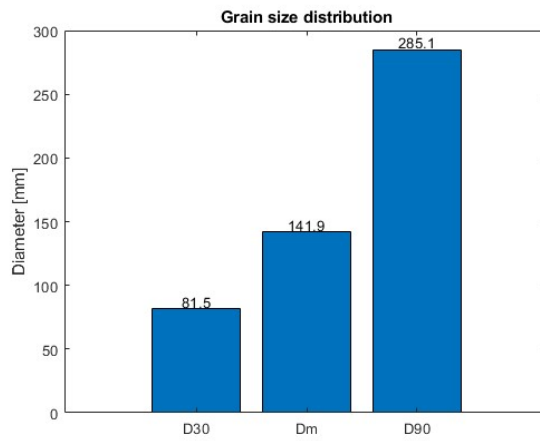


Figure 23: GSD of photo 900901



Figure 24: Photo 900906

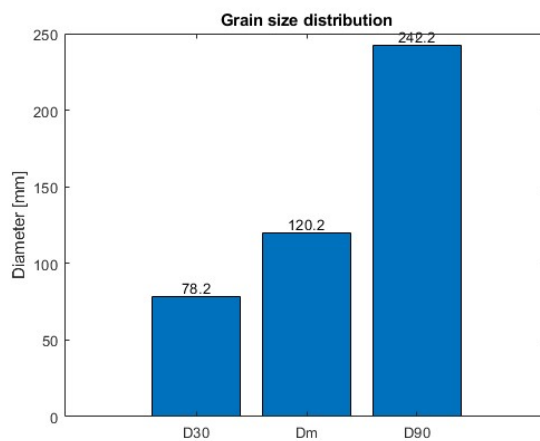


Figure 25: GSD of photo 900906



Figure 26: Photo 900912

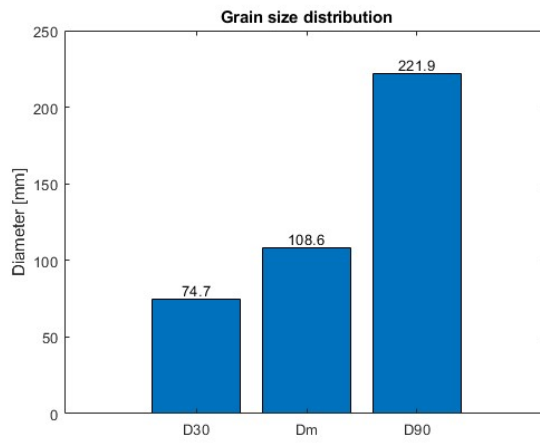


Figure 27: GSD of photo 900912

Then, according to the previous figures, if one averages the results the value for mean diameter is corresponds to $D_{50} = 0.123 m$.

6.2 Hydrology

In order to perform the parabolic method, are going to be considered two main points for the hydro-logical data. The first one is the time scale at which it will be expected the normalization of the mean slope of the river. According to previous studies, this time scale highly depends on the height of the sediments accumulated upstream [17]. Therefore, it was assumed that, roughly each meter of deposition of material in the riverbed is equivalent to a time scale of one year.

Then, having an average elevation of the sediments retained upstream the dam equal to 315.19 *m.a.s.l.* and, knowing that the mean slope of the reach is 5‰ one can estimate that the average elevation of the original bed of the river in the closest point to the dam is around the 311 *m.a.s.l.*, the difference between these two elevations is four meters which means five years may be this mentioned time scale. In any case, to confirm, the effects at ten years time scale are going to be assessed.

The second point to be considered is a moving window of the daily time series of Fig. 3 with the size already set in the first point (five and ten years) in order to avoid the interruption of the hydro-logical data at the window's limits. In simpler words, windows were considered in the next way: year 1 to 5, years 2 to 6, year 3 to 7, year 4 to 8, ..., etc. In such manner year 5 is limit year in the first window but not in the second and so on. Consequently, as the available data starts from year 2005 and ends in year 2023, there are 13 windows to perform the five years window simulation and 9 windows to perform the 10 years window simulation.

6.3 Digital terrain model

The information regarding the elevation in the area of study covers a length of approximately 3 kilometers of Trebbia river surveyed by drone in June 2023. In order to obtain the data of the actual terrain, that is to say, excluding the height of the trees, bridges and some other obstacles, was in the need to perform a classification following a segmentation of the points cloud. Classifying the points allowed to remove those ones that give incorrect information about the real elevation of the terrain. Therefore, the point cloud was classified and segmented in the following classes:

- Wet areas (Blue)
- Dry areas (Dark green)
- Vegetation (Light green)
- Banks (Orange)
- Logs – Trunks
- Dam

An example of this classification can be seen in the following figures. On the left side is displayed a section of the original point cloud, while on the right side, is the same section of the cloud, this time segmented.



Figure 28: Cloud of points (500 m downstream the dam)

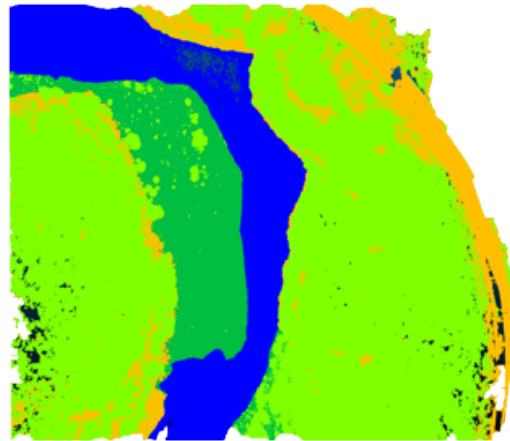


Figure 29: Segmentation of the cloud

Lastly, in order to get the final DTM, vegetation points and logs were deleted whereas the empty spaces were filled by interpolating the surface with the closest points. At the end, a DTM of resolution grid of 10x10 cm was obtained. In the next figure, cells with the highest elevations are represented in red color, and with blue the lowest ones. In the color bar are also displayed the frequency of the elevations where cells surrounding 307 *m.a.s.l.* are the most frequent and, 291 *m.a.s.l.* is the least frequent. Moreover, on the top of the DTM can be seen two red dotted lines which represent bridges, while in the bottom of the

figure can be observed a sudden change in the riverbed from light green to a darker green where the dam is situated (yellow line).

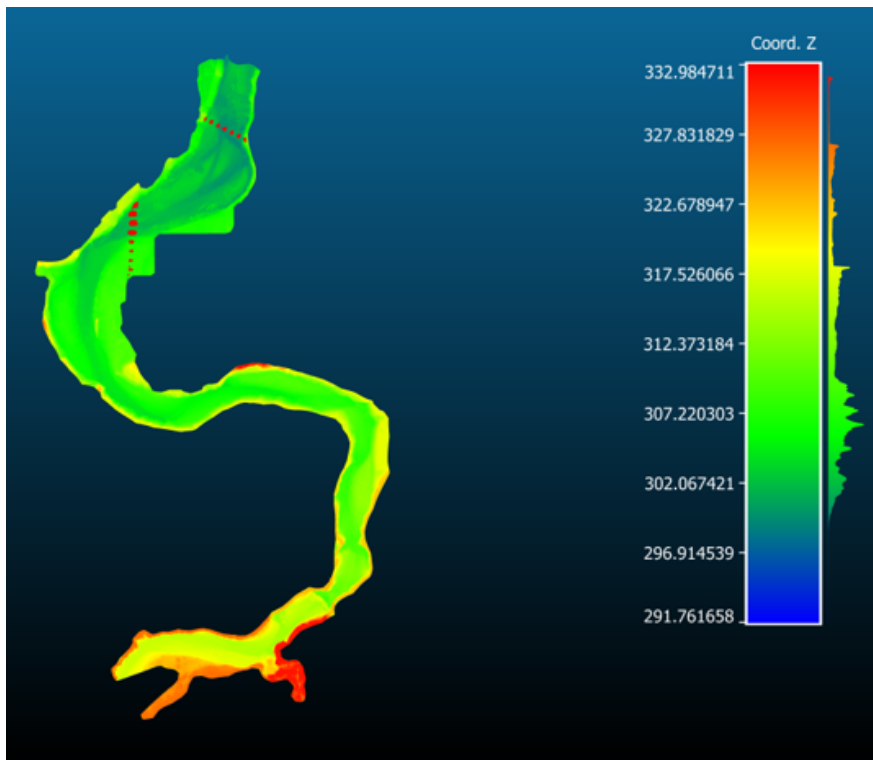


Figure 30: Digital terrain model for the reach of interest (3km)

Once having the DTM, were sampled 111 transverse sections, that is to say in average each 30 meters. This last with the purpose of transforming the three dimensional data into one dimensional data by averaging the elevation of each section in order to obtain one single value representing the elevation of each transverse section along the reach.

Previous field observations carried out in the United States, where a dam was built [10], have shown that degradation effects due to sediments trapping can extend kilometers downstream the dam. Therefore, a coarser DTM was used to cover a larger length beyond the reach both for downstream and upstream. The mentioned DTM comes from a drone survey performed in the year 2015 by the researchers of department of environment, territory and infrastructure from the Polytechnic of Turin. The DTM has a cell resolution of 1M x 1M and was useful to cover three more kilometers upstream the reach of interest and around five kilometers downstream, accounting for a total length of 11.7 km.

In this case, from the coarser DTM were taken another 51 sample sections approximately each 150 meters, and its was performed the same approach. As result of merging the DTM's it was obtained the averaged profile for the total length of 11.7 km.

Finally, the same month of June of 2023, was performed a bathymetry within the pool downstream the dam to know more precisely the depth and shape of the bottom. For the surveyed sections was performed the same process of transverse averaging each of them, thus refining the DTM in one of the most important points.

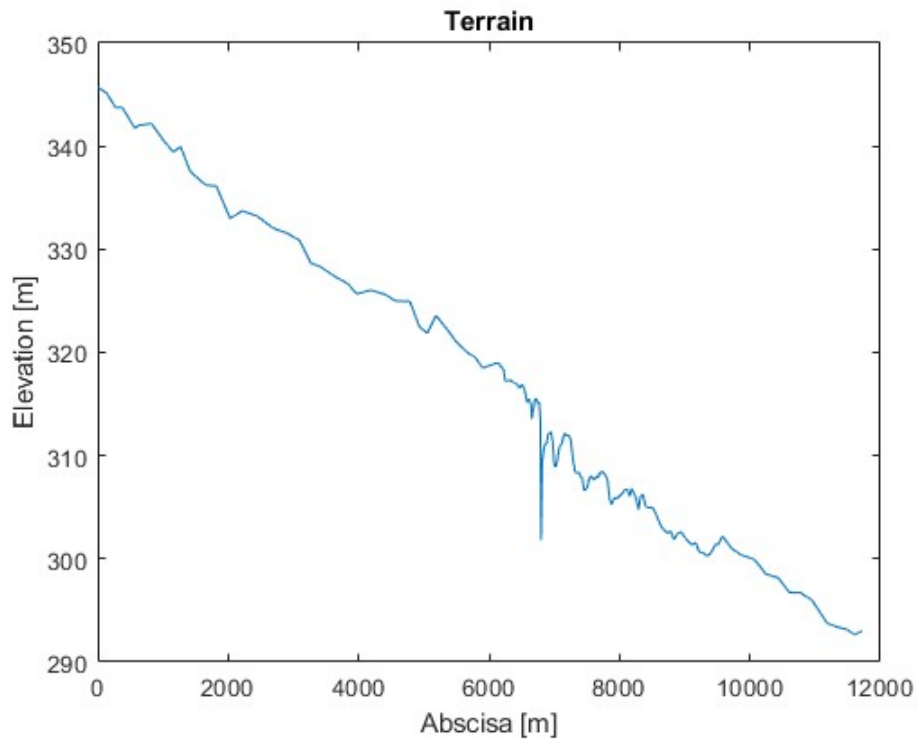


Figure 31: Mean profile of the reach of study

In Fig. 31 it was implemented a local reference system where $x = 0 \text{ m}$ is the point of the first cross section from the coarse DTM, located at 530600.970 E 4951394.693 N and, at $x = 11726 \text{ m}$ is found the last cross section of the coarse DTM at 530843.893 E 4957834.930 N. Similarly, the finer DTM commence at $x = 6140 \text{ m}$ at 530037.787 E 4954022.330 N and finishes at $x = 9508 \text{ m}$ at 530330.593 E 4956014.383 N. Last but not least, the dam is situated at $x = 6770 \text{ m}$ at 530587.770 E 4954400.964 N.

6.4 Inputs for the simulation

In order to apply the parabolic method is needed to set input parameters such as, the initial slope, physical properties of the river and the boundary conditions. First of all, the initial slope is taken from the profile of the terrain, in this case, the mean slope of the reach is equal to 5.5‰.

Regarding the physical properties of the riverbed material, apart from the mean diameter, in order to apply sediment transport theory are needed the porosity and the density of the material. According to the literature, the porosity for gravel rivers is $p = 0.2$ [9]. The submerged relative density for quartz is $\Delta = 1.65$ [9].

Assuming Engelund and Hansen formula Eq. 7, factors Γ and a become: $\Gamma = 0.05C^2$ and $a = \frac{5}{2}$. Therefore, Eq. 23 the PDE to be solved becomes:

$$\frac{\partial \eta}{\partial t} = -\frac{4}{7}F \left(-\frac{\partial \eta}{\partial x} \right)^{7/4} \quad (32)$$

where F is reduced to the following terms thus: $F = 0.05C^2 * \left(\frac{1}{(1-p)} \right) * \sqrt{\Delta g D_{50}^3 \frac{7\Omega}{10} \Omega^{\frac{5}{2}-1}}$

Additionally, in order to solve the second degree partial differential equation are needed one initial condition and two boundary conditions.

For the initial condition, is needed the actual topography of the river extracted from the DTM already displayed in Fig. 17 which is also in table form reported in the Annex 1: River's topography. Regarding the boundary conditions, for the right boundary as well for the left boundary, the sediment transport flux must be equal to zero $f|_{x=0} = 0$ and $f|_{x=L} = 0$. For this purpose, the boundary condition must be set far away from the reach of interest, that is why the total length of the reach for the simulation was set to 11.7 km, while the reach of interest is only made of 3 km, located from kilometer 6 to kilometer 9.

For the reach of interest, and the sections obtained in subsection 6.3 , was calculated the mean breadth taking into account only the active channel including the bars. In this sense, the mean breadth for the analysis is equal to $B_{mean} = 76.05 \text{ m}$.

7 Results

In order to perform a conservative approach, that is to say, to guarantee that the first flush of sediments will be the largest possible, it was considered the following hypothesis. The first one is assuming that the dam will be instantaneously removed. Although this hypothesis is almost impossible to happen, it guarantees that the deposited sediments are not progressively dragged as it would happen when the dam altitude becomes lowered due to a gradual demolition.

The second one is not to contemplate the presence of the by-pass, which is the one allowing the low flows to pass through it, in other words, we are deviating the flow to the main channel (where the dam is), which means all the time series of flow rate will contribute to the calculation of the sediment transport within the main channel.

The third one, is that sediment transport will occur only when the shield stress is larger than 0.03 ($\tau^* > 0.03$), threshold value corresponding to the movement of gravels [9]. According to Dietrich relationships (1982) the Reynolds particle number is calculated as following:

$$Rp = \frac{\sqrt{\Delta g D D}}{\nu} \quad (33)$$

where:

Δ : is the submerged relative density previously mentioned in last subsection.

g : is the gravity acceleration.

D : is the mean diameter.

By evaluating this expression one gets a value of the Reynolds particle number of $Rp = 173,554$. As the value is larger than 10,000, the value of the shield stress tend to be 0.03 [9].

7.1 Evolution of the mean profile

The simulation was run using the time series of discharge described in subsection 6.2, details of the code used to perform the simulation is listed in the Annex 2: Main code. The first flush of sediments, also the strongest, occurs when the discharge is larger than $Q = 197.57 \text{ m}^3/\text{s}$, flush which graphically speaking almost fill the pool downstream the dam. A discharge like this one producing the beginning of sediment transport can be exceed twice a year according to the flow duration curve of Fig. 5. This flush occurs normally within two years in all of the windows and impose more or less the same first great change in the profile.

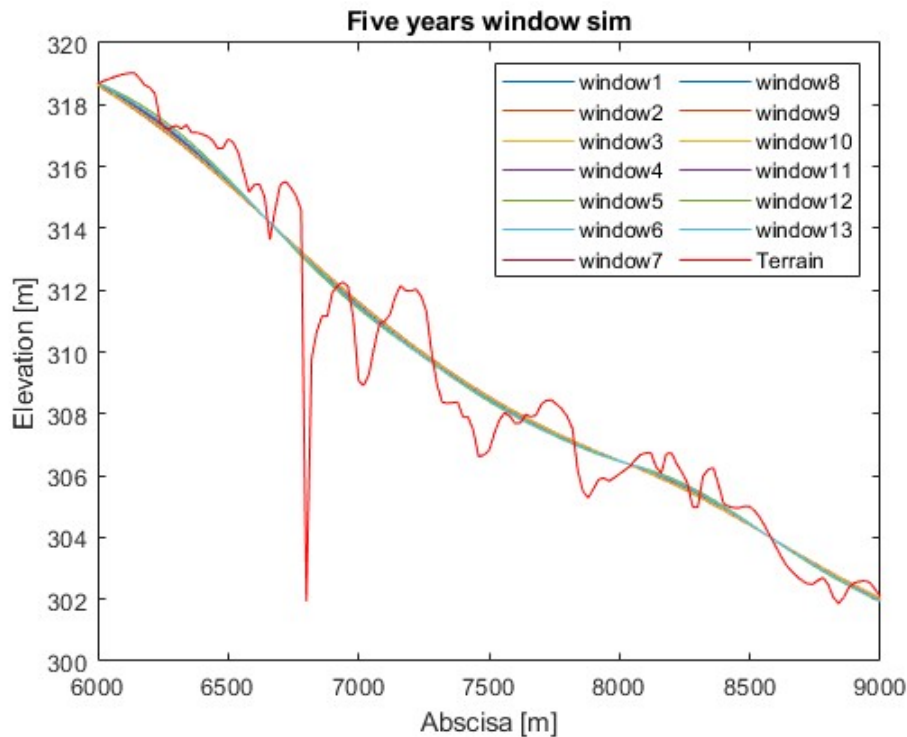


Figure 32: Migration of the profile for the different time series windows

The estimated final configuration of the profile, was computed as the mean profile of the thirteen simulations for the five years windows Fig. 33 and, as the mean out of the nine simulations of ten years windows and Fig. 35. The details of the code used to perform the simulation is listed in the Annex 3: Results processing code

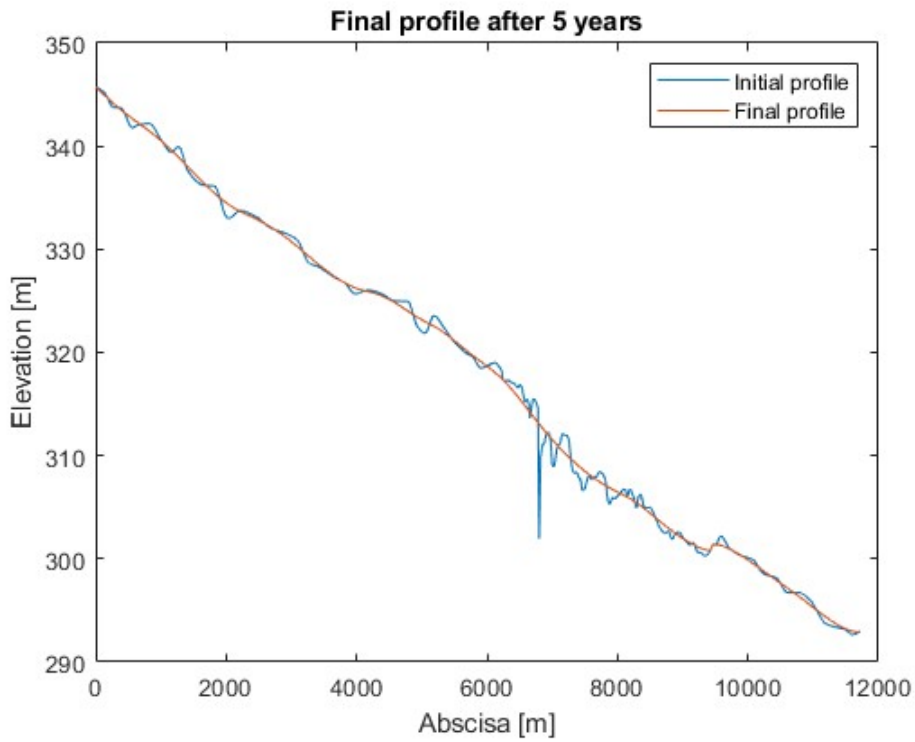


Figure 33: Estimated profile after 5 years

The final profile shows that the pool is full with sediments and the one dimensional bars are almost depleted along the longitudinal profile. In general terms, at the end of the period of five years the river has recovered its natural slope.

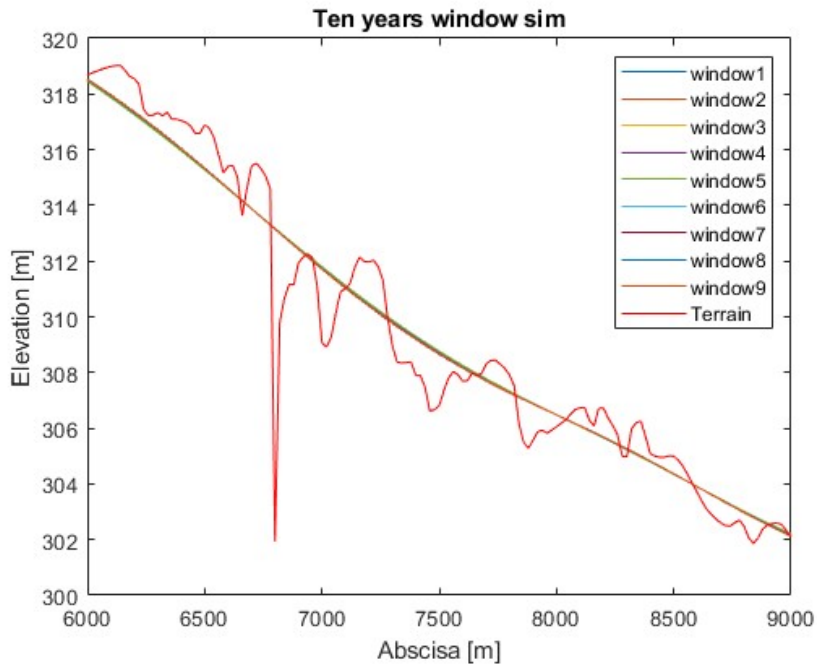


Figure 34: Migration of the profile for the different time series windows

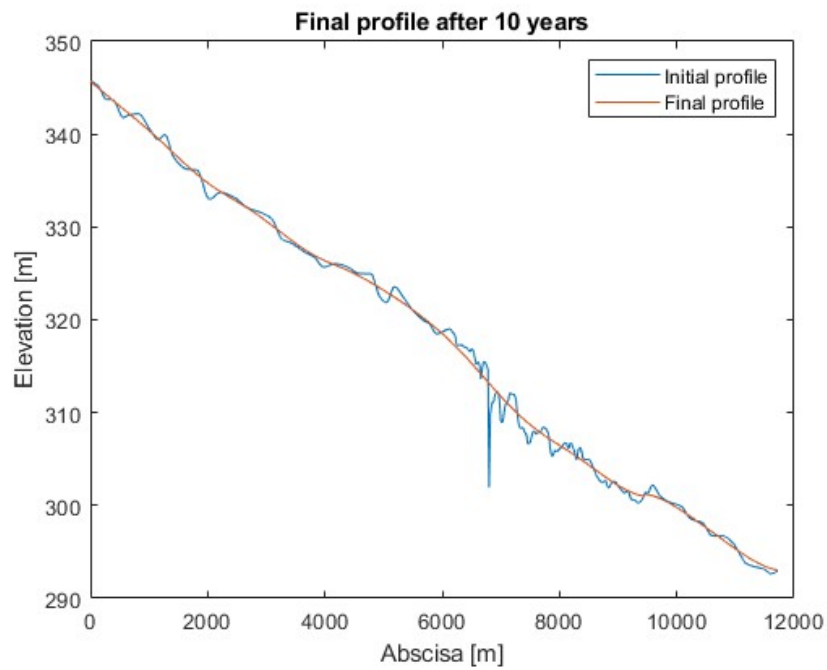


Figure 35: Estimated profile after 10 years

Similar case occurs in the ten years simulation because as seen in Fig. 33 and Fig. 35, the resulting profiles after five and ten years do not have significant differences between each other. This leads to say that the major changes occurs before five years after the dam removal, although the final profiles of the five years window simulations Fig. 32 display larger variability with respect to the ten years windows simulations Fig. 34 which almost all profile lines seems to tend to the same profile trajectory.

7.2 Volume of the pool

In June 2023 it was performed a bathymetry for the lake immediately after the dam which is one of the most interesting points of the terrain as it is expect it to be the one with more degradation. The result of this survey can be seen in Fig. 36 where the level of the water is displayed in yellow color.

From the year of its construction up to these days the bottom of the lake downstream the dam has been degrading reaching a mean elevation of 301.82 *m.a.s.l.*, whereas the bottom is found at 9.76 *m* below the water level in its deepest point. If one takes the estimated initial elevation of the river 311 *m.a.s.l.* and subtracts the mean actual elevation one finds a total scouring of 9.18 *m*, which means an average scouring rate of 10 *cm/year*. This last value might see low but it is important to remind that almost all the water within the river passes through the bypass built by the time of the construction of the dam. At the same time the scouring was occurring downstream, deposition of material was taking place upstream the dam reaching an average elevation of 315.19 *m.a.s.l.*.

The computation of the volume of the 3D figure in Fig. 36 for a step of $dz=0.1$ m, is calculated by numerical integration.

$$V_{pool} = \sum_{limz=0.1}^0 \left(\sum limz - [vq] \right) \Delta x \Delta dy \quad (34)$$

valid for values of $[vq]$ fulfilling $limz < [vq]$ in every step.

where:

$limz$: is a vector with depth values going from the minimum depth (-9.76 m) to zero.

$[vq]$: is a matrix with depth surveyed values.

Δx and Δy : the chosen discrete interval equal to 0.1 m.

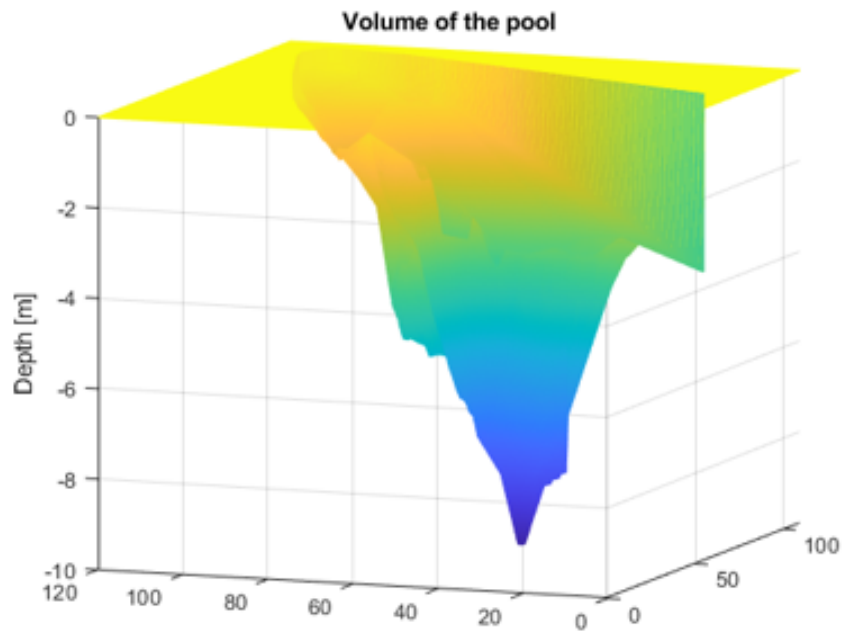


Figure 36: 3D view of the pool survey

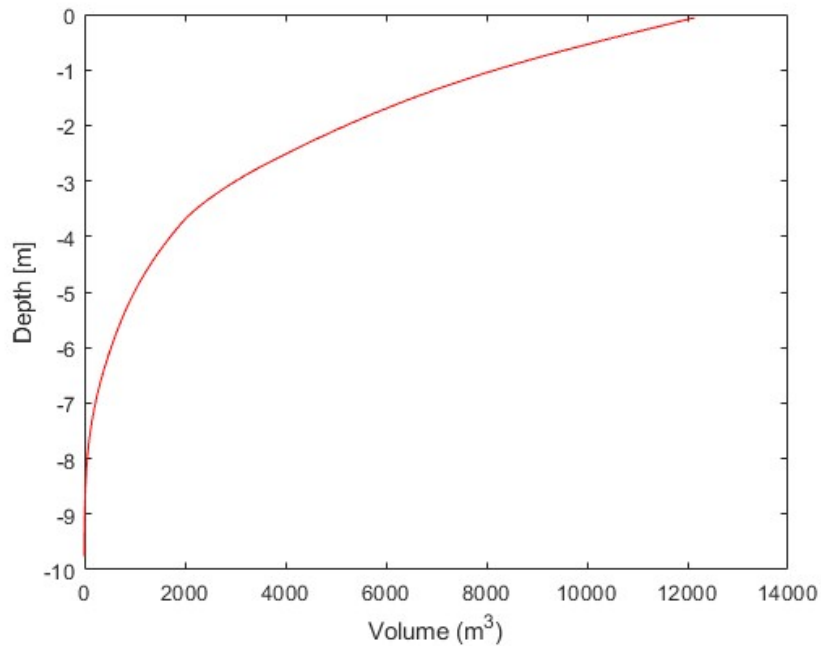


Figure 37: Volume curve of the pool

The total volume of the pool downstream the dam is equal to 12143.15 m^3 , while the volume of water corresponding to each meter of depth of the pool is displayed in Fig. 37

7.3 Volume transported downstream the dam

In order to compute the expected volume of sediments transported from upstream the dam, it was considered a influence length of 500 m. In upstream direction, 500 m after the dam can be found the first meander, that is why this interval was taken.

Consequently, for each variation of the profile it was calculated the area between the initial profile and the final profile in Fig. 33 and Fig. 35 modified by the time series of discharge. By multiplying by the mean width of the river it was obtained the time series of mobilized volume from the upstream to the downstream side. In the following figures, from one side is displayed the transported sediments for each time step Fig. 38 whereas, Fig. 39 shows the accumulated volume in tn the time series.

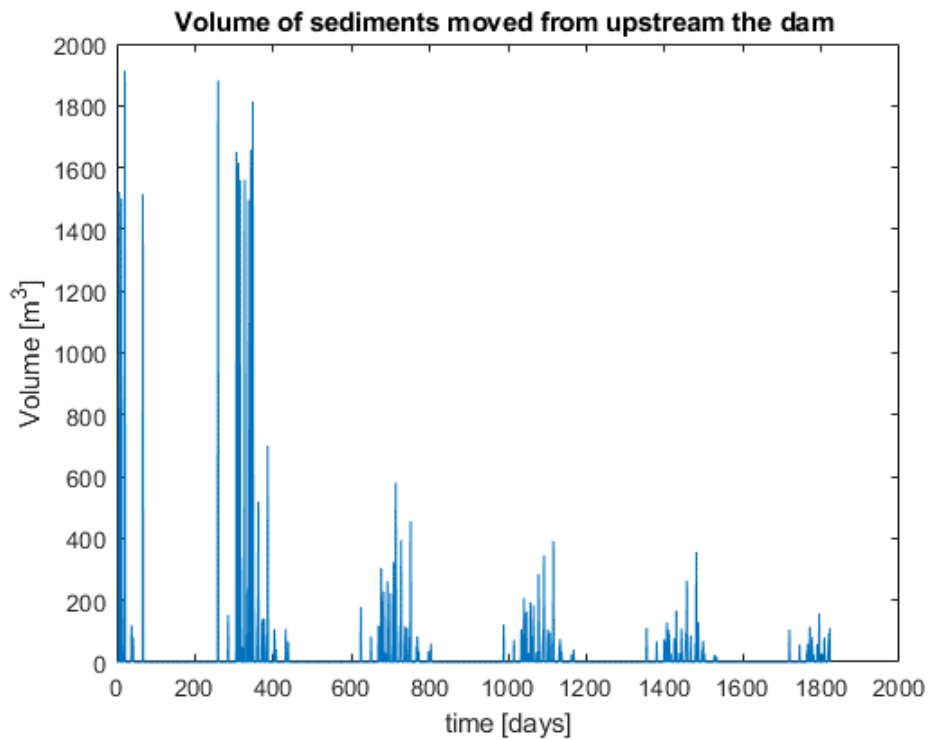


Figure 38: Time series of volume of transported sediments

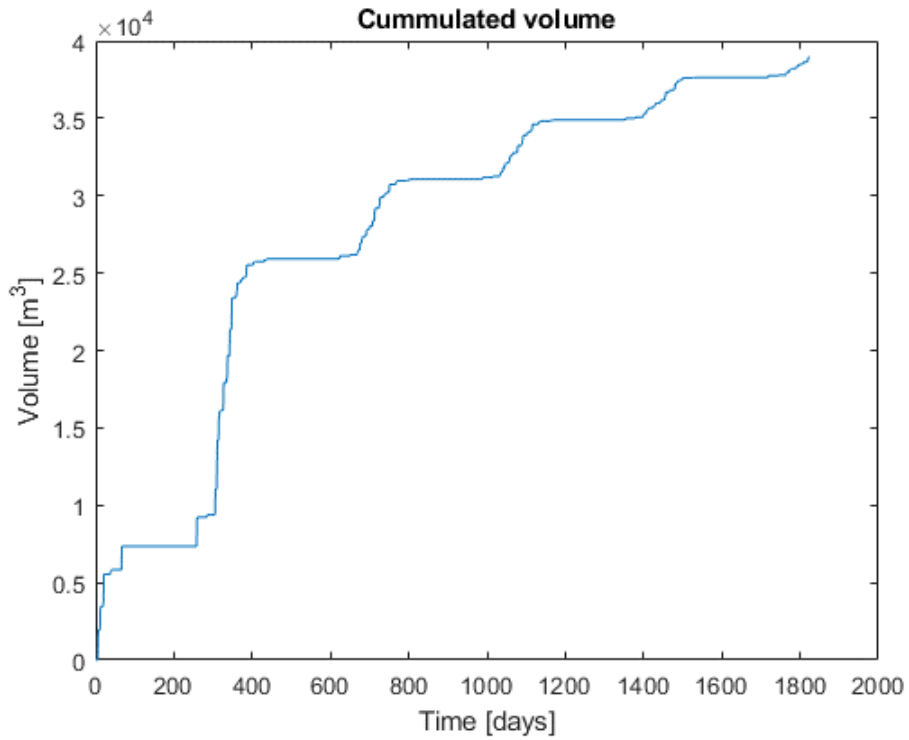


Figure 39: Accumulated volume within a five years window

The total sediment transport volume after five years is $38946m^3$. The volume of transported sediments is decreasing in time since the the availability of them is lowered by the passage of flow over the years while in the meantime the river is recovering its natural slope. Moreover, the largest pulse of sediments accounts for $1913.3m^3$, which is 15.75% of the total volume of the pool and 4.91% of the total transported volume.

From Fig. 39 it is easy to appreciate that the largest amount of sediment transport ($18176 m^3$) took place between 250 and 400 days of the simulation.

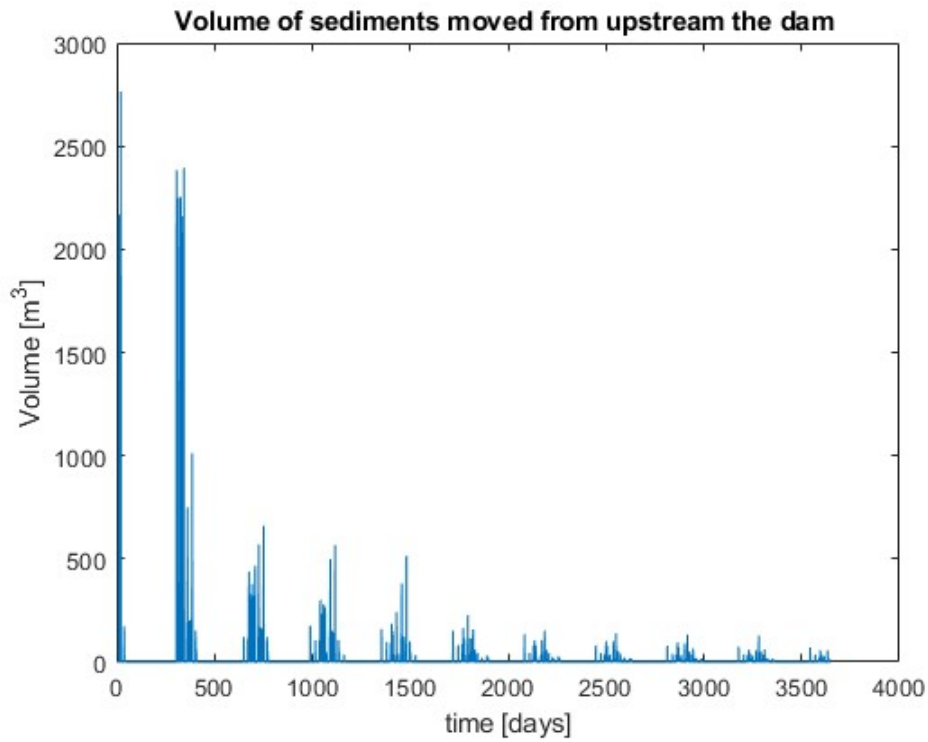


Figure 40: Time series of volume of transported sediments

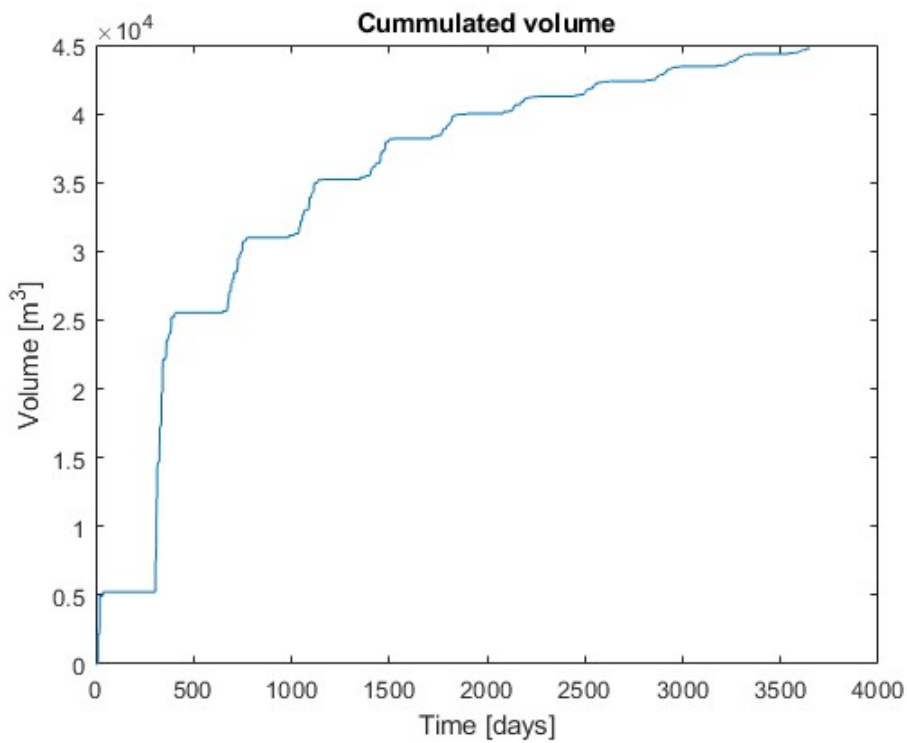


Figure 41: Accumulated volume within a ten years window

The total sediment transport volume after ten years is $44753.3m^3$. The volume of transported sediments is decreasing in time since the the availability of them is lowered by the

passage of flow over the years while in the meantime the river is recovering its natural slope. Moreover, the largest pulse of sediments accounts for $2763.5m^3$, which is 22.76% of the total volume of the pool and 6.17% of the total transported volume.

Similarly, as occurred in the five years window simulation, the largest amount of sediment pulse in this case is found within the same period of time 250-400 days and accounts for $20297.34 m^3$. For the both simulations, after four hundred days almost all the upstream available sediments are consumed.

8 Conclusion

Another look to the results of Fig. 33 can be noticed when plotting the difference in elevation between the actual simulated profile against the initial profile in a $XvsT$ plot like in Fig. 42. This was useful to plot the spatial-temporal evolution of the bed to determine up to what period of time the changes of the bed could be significant.

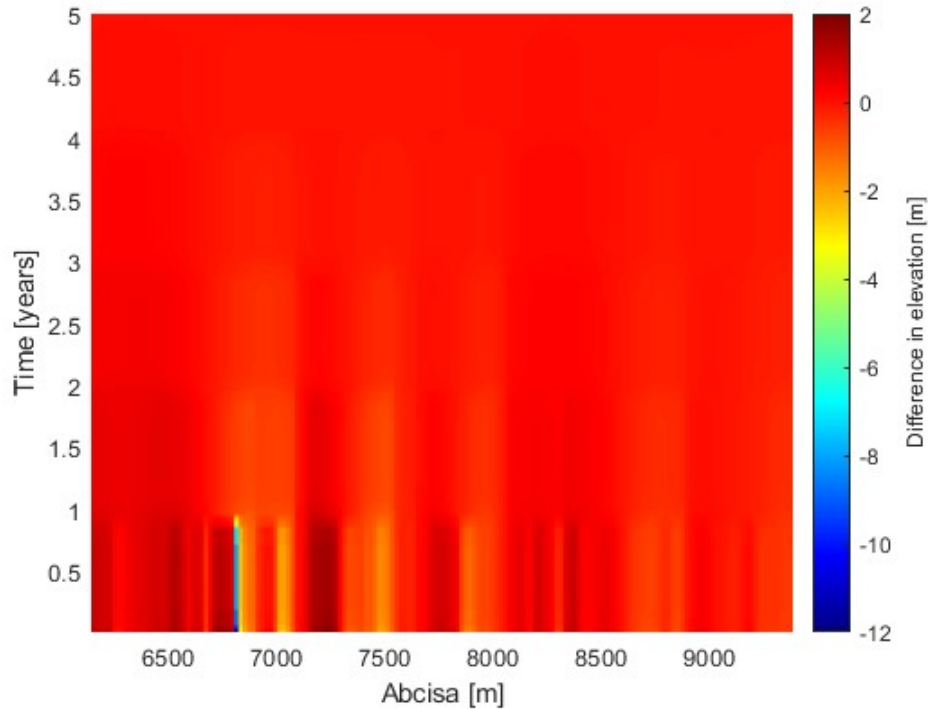


Figure 42: Change of river's bed elevation throughout the years

In Fig. 42 the pool after the dam is represented in color blue in the bottom of the figure in the abscissa 6800 m. That point exhibits the largest difference with respect to the final profile accounting for approximately 9 m of difference, which after one year of simulation is almost dissipated (Aggradation). Dark spots represents longitudinal bars located in abscissas 6000 m to 6500 m and 8000 m to 8500 m, which slowly disappear before four years (Degradation). From the same figure, yellow to orange colors are the one determining up to what period the changes in the bed are significant, this situation occurs within four years of simulation.

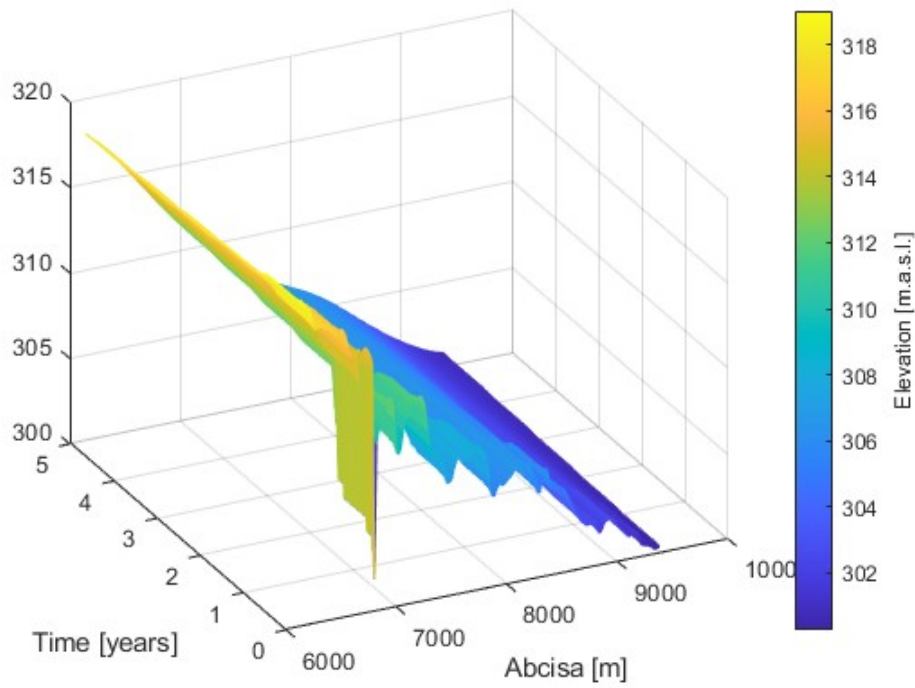


Figure 43: 3D-view of the evolution of the bed after five years

From the 3-D view of Fig. 43 is also noted that the major changes occur within one year of simulation. Same results are plotted for the ten years window simulation:

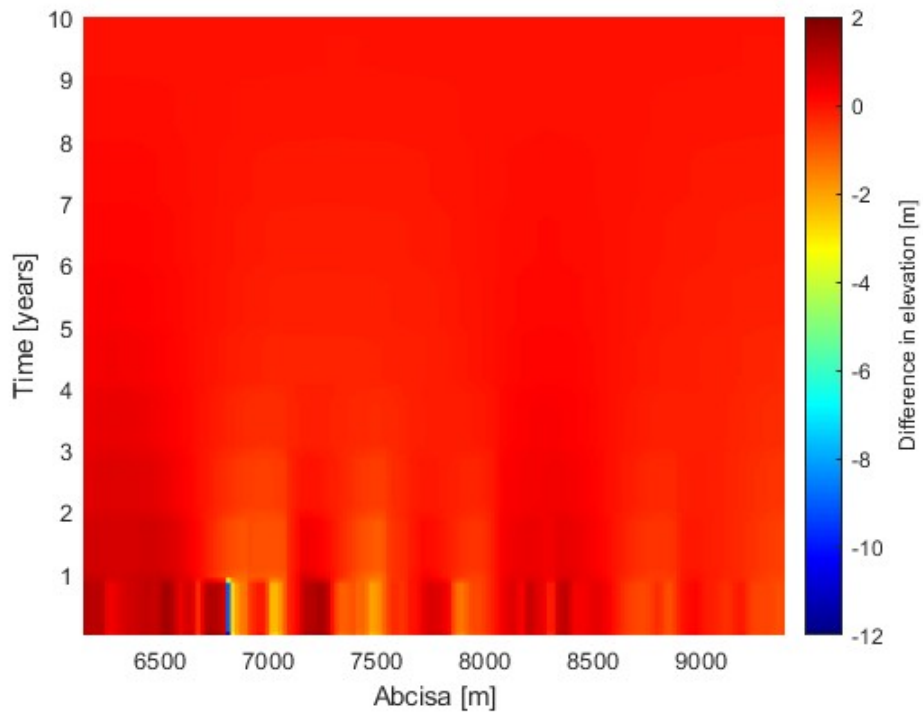


Figure 44: Change of river's bed elevation throughout the years

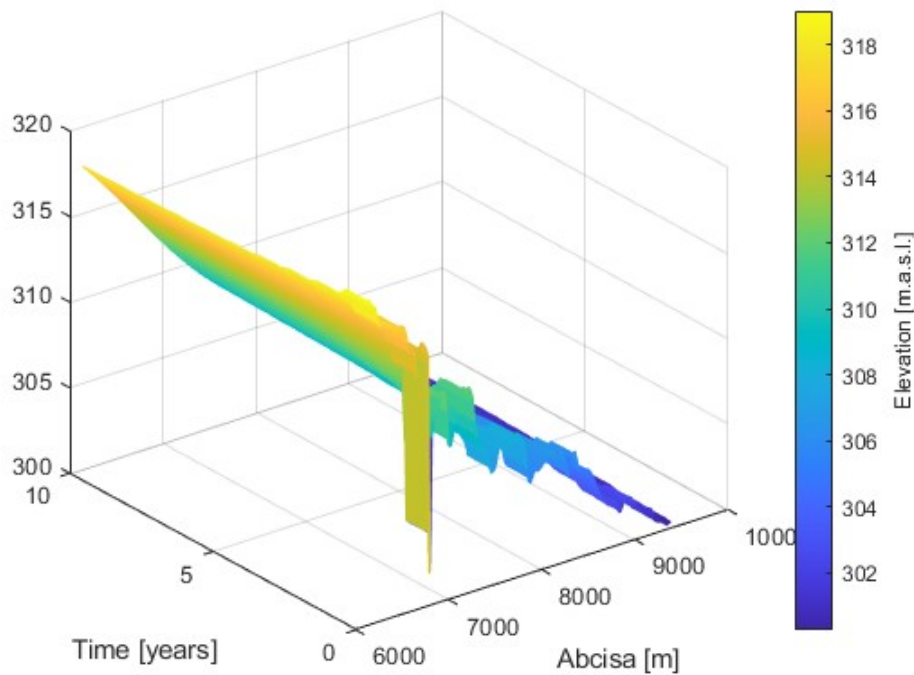


Figure 45: 3D-view of the evolution of the bed after ten years

Similar consequences occur when simulating the ten years window of discharge time-series, except for the longitudinal bars found in abscissas 6000 m to 6500 m which tend to be present up to five years after the removal. These results the relative fast recovering of the rivers bed are congruent with the measurements in field made by the researches in other latitudes like [17] and [30] or what ORG's reported like in [23].

It is important to note that the recovery of the natural slope will depend also in which time of the year begins the demolition. For this simulation was assumed that the hydrological time series begins with the calendar year, but it was shown before that the most important contributions to the sediment transport take place during the Autumn months. Therefore, if civil works of the demolition are planned during the dry period (summer), the first pulse of sediments will occur within period of few months, thus reducing a couple of months the total time spent for the river to recover.

It is also important to remark that the simulation was performed using the mean daily data recorded by the gauge which do not exhibits the peaks of flood events. Consequently, the presence even of a five years return period event will be capable of moving much more sediments at once in comparison to the peaks of the mean daily discharge time series. However, if this occurs, in the less conservative scenario 31.18 % of the expected amount of sediments to be mobilized from upstream the dam, would be trapped in the pool. In the most conservative scenario, assuming that all available sediments would be dragged to the reach of Trebbia within the downtown of Bobbio, the risk of flood will not be increased significantly due to the raise of the rivers bed in 3.6 cm [2]. This comes as result of the hydrodynamic simulation of 200 years return period flood, where the flooded area accounts for 1062481.69 m^2 and it was assumed that all moved sediments were deposited all over that area.



Figure 46: 200 years return period flood mapping in the nearby of Bobbio town

This preliminary study can lay the foundation for other more detailed studies regarding the topic of habitat in order to determine the diagnosis of the river and to assess the conditions before the removal to estimate the behavior in the post removal scenario. Moreover, the possible modifications in the landscape bedforms can be assessed through a 2D morphodynamic simulation. Economical aspects such as, cost of the demolition and possible tourism incomes or losses should be also considered, in this way, to have a entire scientific spectrum to assess the possible removal.

9 Annex 1: River's topography

Table 4: River's topography for the simulation

Count	River Station	Distance [m]	Abscissa [m]	Elevation [m.a.s.l.]
1	13639	0	0	345.72
2	13503	135.6	135.6	345.15
3	13365	138.1	273.7	343.75
4	13259	106.5	380.2	343.73
5	13072	187.7	567.9	341.74
6	13014	57.6	625.5	342
7	12815	199	824.5	342.19
8	12630	185.2	1009.7	340.55
9	12482	148.1	1157.8	339.43
10	12368	114	1271.8	339.95
11	12220	147.7	1419.5	337.53
12	11981	238.9	1658.4	336.21
13	11823	158.5	1816.9	336.14
14	11610	213.2	2030.1	332.99
15	11420	189.8	2219.9	333.73
16	11192	228.3	2448.2	333.2
17	10953	239.3	2687.5	332.05
18	10740	212.9	2900.4	331.57
19	10546	194.3	3094.7	330.86
20	10372	173.9	3268.6	328.67
21	10218	154.1	3422.7	328.27
22	10008	209.5	3632.2	327.39
23	9814	194.5	3826.7	326.69
24	9666	148.1	3974.8	325.67
25	9457	208.9	4183.7	326.04
26	9236	221.1	4404.8	325.63
27	9076	159.8	4564.6	325
28	8855	221.3	4785.9	324.95
29	8707	147.7	4933.6	322.49
30	8587	120	5053.6	321.86
31	8456	130.7	5184.3	323.57
32	8303	153.4	5337.7	322.42
33	8138	164.8	5502.5	320.98
34	7968	170	5672.5	319.98
35	7859	108.9	5781.4	319.56
36	7737	122.2	5903.6	318.49
37	7498	236.7	6140.3	319.03
38	7475	23	6163.3	318.82
39	7452	22.5	6185.8	318.59
40	7434	18.5	6204.3	318.53
41	7413	21.3	6225.6	318.24

42	7392	20.9	6246.5	317.24
43	7364	28.3	6274.8	317.23
44	7343	21.2	6296	317.34
45	7322	21.1	6317.1	317.21
46	7303	19.2	6336.3	317.36
47	7277	26.1	6362.4	317.09
48	7251	25.9	6388.3	317.1
49	7229	22	6410.3	316.99
50	7207	22.3	6432.6	316.96
51	7185	21.7	6454.3	316.58
52	7160	24.7	6479	316.59
53	7135	24.7	6503.7	316.91
54	7113	22.1	6525.8	316.7
55	7092	21.3	6547.1	316.25
56	7056	36.1	6583.2	315.15
57	7030	25.5	6608.7	315.5
58	7005	25.2	6633.9	315.2
59	6995	10.2	6644.1	314.82
60	6982	13	6657.1	313.56
61	6968	13.8	6670.9	314.32
62	6951	17.4	6688.3	314.84
63	6938	13.6	6701.9	315.45
64	6925	12.8	6714.7	315.53
65	6903	22.4	6737.1	315.37
66	6886	17.2	6754.3	315
67	6870	16.1	6770.4	315.19
68	6853	16.8	6787.2	313.4
69	6841	11.6	6798.8	301.82
70	6825	16	6814.8	309.33
71	6799	26.2	6841	310.7
72	6777	22	6863	311.18
73	6756	21	6884	311.15
74	6736	19.7	6903.7	312.04
75	6713	23.1	6926.8	312.18
76	6690	23.2	6950	312.3
77	6664	25.9	6975.9	311.38
78	6637	27.2	7003.1	308.98
79	6620	17.5	7020.6	308.91
80	6594	26	7046.6	309.49
81	6581	12.6	7059.2	310.14
82	6557	24.5	7083.7	310.96
83	6530	26.9	7110.6	311.03
84	6504	26.4	7137	311.7
85	6479	25.4	7162.4	312.15
86	6453	25.8	7188.2	311.93
87	6426	26.8	7215	312.04
88	6387	38.8	7253.8	311.53

89	6354	33.5	7287.3	309.57
90	6320	34	7321.3	308.37
91	6294	26.5	7347.8	308.34
92	6263	30.5	7378.3	308.39
93	6239	24.1	7402.4	307.89
94	6212	27	7429.4	307.89
95	6185	27.1	7456.5	306.61
96	6145	40.4	7496.9	306.77
97	6110	35.2	7532.1	307.67
98	6077	32.5	7564.6	308.05
99	6047	30.3	7594.9	307.73
100	6031	15.7	7610.6	307.64
101	5995	36.5	7647.1	308.01
102	5972	23.2	7670.3	307.83
103	5946	26.4	7696.7	308.28
104	5910	35.6	7732.3	308.46
105	5881	28.9	7761.2	308.29
106	5848	32.6	7793.8	307.99
107	5823	25.4	7819.2	307.53
108	5794	29.3	7848.5	305.75
109	5763	30.6	7879.1	305.28
110	5732	30.8	7909.9	305.73
111	5711	21.3	7931.2	305.98
112	5688	23.5	7954.7	305.81
113	5663	24.8	7979.5	305.93
114	5631	32.1	8011.6	306.13
115	5602	29.1	8040.7	306.31
116	5561	41.4	8082.1	306.68
117	5525	35.9	8118	306.75
118	5488	36.8	8154.8	306.03
119	5455	32.8	8187.6	306.82
120	5417	38.4	8226	306.27
121	5386	30.5	8256.5	305.85
122	5351	34.9	8291.4	304.77
123	5318	32.6	8324	306.06
124	5284	33.8	8357.8	306.26
125	5240	44.1	8401.9	305.07
126	5193	47.3	8449.2	304.95
127	5151	42.1	8491.3	305.02
128	5118	33.4	8524.7	304.8
129	5082	36.5	8561.2	304.3
130	5047	34.7	8595.9	303.75
131	4994	53.3	8649.2	303
132	4908	86.4	8735.6	302.48
133	4864	44.4	8780	302.7
134	4806	57.8	8837.8	301.86
135	4750	56.1	8893.9	302.51

136	4698	52.2	8946.1	302.6
137	4642	55.8	9001.9	302.07
138	4590	51.9	9053.8	301.68
139	4536	54	9107.8	301.33
140	4476	60.5	9168.3	301.58
141	4425	51	9219.3	300.7
142	4342	82.7	9302	300.49
143	4303	38.8	9340.8	300.26
144	4250	53.2	9394	300.49
145	4210	40	9434	300.94
146	4170	39.8	9473.8	301.46
147	4136	34.3	9508.1	301.31
148	4060	72	9580.1	302.19
149	3918	141.6	9721.7	300.99
150	3770	148	9869.7	300.37
151	3569	201.4	10071.1	299.92
152	3397	172	10243.1	298.53
153	3207	190.5	10433.6	298.16
154	3036	171.5	10605.1	296.73
155	2868	167.9	10773	296.72
156	2685	182.9	10955.9	295.97
157	2590	95.4	11051.3	295.02
158	2456	133.9	11185.2	293.74
159	2300	156.3	11341.5	293.38
160	2158	142.4	11483.9	293.16
161	2038	120.2	11604.1	292.65
162	1916	121.9	11726	293.03

10 Annex 2: Main code

```
clear all
close all

% 1. Inputs
global S0 D50 K Eta0 L tempinicond fitresult2 fitresult3

Sbh=0.0055; % Slope at bankfull discharge
S0=Sbh; % Initial slope
D50= 0.122; % [m] mid grain size diameter
g=9.81; % [m/s^2] gravity constant
p=0.2; % porosity for gravel rivers
L=11726; %[m] reach length
delta=1.65; %submerged relative desnsity for quartz
T=365; % [days] time of analysis
bmean=76.05;

load var.mat
%%%%%% 2.1. Plot of discharge raw data %%%%%%%%%%%%%%%
figure (1)
plot(Dates,Q)
title("Trebbia river at Bobbio")
ylabel("Discharge [m^3/s]")

mean1=mean(Q,'omitnan');
%%%%%% 2.2. Only considering data from 02/01/2005 %%%%%%%%%%%%%%%

Dates2=Dates(16073:end);
Q2=Q(16073:end);
Threshold=0;% [m^3/s] Threshold value for the bypass
Q3=NaN(length(Q2),1);
Q3(find(Q2>Threshold))=Q2(find(Q2>Threshold));
figure (2)
plot(Dates2,Q2)
% hold on
% plot(Dates2,Q3)
title("Trebbia river at Bobbio")
% ylabel("Discharge [m^3/s]")
mean2=mean(Q2,'omitnan');
hold on
Qmean=mean2; % mean discharge [m^3/s]
yline(Qmean,'r',"Label",[num2str(Qmean) ' m^3/s'])
% legend('Time series of discharge','Values above the threshold')
saveas(gcf,'figure6_1','jpg')

%%%%%% Mean annual discharge %%%%%%%%%%%%%%%
```

```

for i=1:length(Q2)
    Qn(i)=isnan(Q2(i));
    if Qn(i)==1
        Q4(i)=Qmean;
    else
        Q4(i)=Q2(i);
    end
end

clear Qn
for k=1:18
    Qn(k)=sum(Q4(((k-1)*365)+1:k*365));
end

Q4mean=mean(Qn);

% for i=1:length(Q2)
%     Qn(i)=isnan(Q2(i));
%     if Qn(i)==1
%         Q4(i)=Qmean;
%     else
%         Q4(i)=Q2(i);
%     end
% end
%
% Q4mean=sum(Q4)/(length(Q2)/365);

Q2(end+1:6633*2)=Q2;

% 3. Plot of the terrain %%%%%%%%%%%

load Terrain.mat

figure(3)
plot(Terrain(:,1),Terrain(:,2))
title('Terrain')
ylabel("Elevation [m]")
xlabel("Abscisa [m]")

%% 4. Fit: Smoothing the terrain by linearinterp and preserving shape
interp

[xData, yData] = prepareCurveData( Terrain(:,1),Terrain(:,2));

% Set up fittype and options.
ft = 'linearinterp';
ft2 = 'pchipinterp';

% Fit model to data.

```

```

[fitresult, gof] = fit( xData, yData, ft, 'Normalize', 'on' );
[fitresult2, gof2] = fit( xData, yData, ft2, 'Normalize', 'on' );

% Plot comparing all smoothing choices
figure(4)
plot( fitresult, xData, yData );
% Label axes
xlabel( 'Abscisa [m]', 'Interpreter', 'none' );
ylabel( 'Elevation [m]', 'Interpreter', 'none' );
title('Terrain smoothing')
grid on
hold on
plot(fitresult2, xData, yData );

% Moving mean smoothing
hold on
M2 = movmean(Terrain(:,2),2);
plot(Terrain(:,1),M2)
hold on
M3 = movmean(Terrain(:,2),3);
plot(Terrain(:,1),M3)
legend('Terrain points', 'Smooth linear', 'Terrain points', 'Smooth curve',
'Moving mean2', 'Moving mean3', 'Location', 'NorthEast', 'Interpreter',
'none' );

%5 Pool of the dam surveyed by the boat %%%%%%%%%%%%%%%

figure %Pool of the dam surveyed by the boat
const=100;
xcoor=Summary.Track(:,1)+const;
y=Summary.Track(:,2)+const;
z=Summary.Depth;
zmean=mean(z);
plot3(xcoor,y,z, ".")
title('Profile in the pool of the dam')
ylabel("y coord. [m]")
xlabel("x coord. [m]")
zlabel("Depth [m]")

sp=0.1;

[xq,yq] = meshgrid(0:sp:120, 0:sp:110);
vq = griddata(xcoor,y,z,xq,yq);

figure
mesh(xq,yq,vq)
hold on
plot3(xcoor,y,z, ".r")

```

```

i1=(find(z>3.091 & z<3.0925));
i2=(find(z>2.3475 & z<2.3485));
i2=i2(1);
i3=(find(z>3.7205 & z<3.7215));
i3=i3(end);
i4=(find(z>2.3285 & z<2.3295));

xcoor(i2:i1)=NaN; xcoor(i3:i4)=NaN;
indx=find(isnan(xcoor)==0);
xcoor=xcoor(indx);
y=y(indx);
z=z(indx);

[xq,yq] = meshgrid(0:sp:120, 0:sp:110);
vq = griddata(xcoor,y,z,xq,yq);

figure
mesh(xq,yq,vq)
hold on
plot3(xcoor,y,z,".r")

vq=-vq;
for i=1:length(yq)
    flag=find(isnan(vq(:,i)));
    vq(flag,i)=0;
end

figure
mesh(xq,yq,vq)
title('Volume of the pool')
zlabel('Depth [m]')

V=[];H=[];dxy=0.1;elev=0; dz=0.1;
Miny=min(min(vq));
for limy=Miny:dz:elev
    vq_Parz=vq;
    vq_Parz(find(vq>limy))=limy;
    V=[V,sum(sum(limy-vq_Parz))*dxy^2];
    H=[H,limy];
end

figure
plot(V,H,'r-')
title('Volume of the pool vs depth')
xlabel('Volume (m^3)');ylabel('Depth [m]');

['The total volume of the pool is ' num2str(max(V)) ' m^3']

culvert=6657;

```

```

reinput=7003;

% 6. Domain for parabolic method %%%%%%%%%%%%%%%%%%%%%%%%%%%%%%%%%%%%%%%%%%%%%%%%%%%%%%%%%%%%%%%%%%%%%%%%%

for iw=1:13%initial window (e.g iw=1 yearsw=5 means:
--> year 1 to 5 iw=2 year 6 to 10)
years=5;% size of window [years] for the simulation
dx=20; % [m] delta in space
dt=1;% days
t=1:dt:365*years;
xspan=0:dx:L; % [m]Interval x of analysis

tday=0:10*60:24*3600;
tempinicond=(fitresult2(xspan)).';t_current=0;
name=['simulation 5 years threshold = 0' num2str(iw)];
sol(1,:)=tempinicond;
time_sol=[0 tempinicond];
save(name,'time_sol');
for i=(iw-1)*365+1:((years+(iw-1))*365)
Q=Q2(i);
%if Q>0
q=(Q-Threshold)/bmean;
if q>0
h=(D50^(1/6)*q/6.74)^(3/5)*(9.81*S0)^(-3/10);
tau=h*S0/(D50*delta);
if tau>0.03
%h=(q/ks)^(3/5)*(S0)^(-3/10);% [m] water depth (simplified approach)
c=6.74*(h/D50)^(1/6); % Conductance
ks=6.74*(1/D50)^(1/6)*sqrt(9.81);
a=5/2;% factor a
gamma=0.05*c^2;% factor gamma
Tc=0;% critical shield stress = 0
A=(q/ks)^(3/5)*(1/(D50*delta)); % [m^2]
K=gamma*(1/(1-p))*sqrt(delta*g*D50^3)*(7*A/10)*A^(a-1);% constant term
sol = pdepe(0,@parab2,@inicond,@bcfun3,xspan,tday);
% We have chosen fitresult2 for the ic.
if Q>Threshold
tempinicond=sol(end,:);t_current=t_current+tday(end);
else
tempinicond=[sol(end,1:culvert) tempinicond(culvert+1:reinput-1)
sol(end,reinput:end)];
end
t_current=t_current+tday(end);
%time_sol=[t_current/86400 tempinicond];
time_sol=[time_sol;t_current/86400 tempinicond];
save(name,'-append','time_sol');
else
tempinicond=sol(end,:);t_current=t_current+tday(end);
time_sol=[time_sol;t_current/86400 tempinicond];

```

```

save(name, '-append', 'time_sol');
end
else
tempinicond=sol(end,:);t_current=t_current+tday(end);
time_sol=[time_sol;t_current/86400 tempinicond];
save(name, '-append', 'time_sol');
end

[xData, yData] = prepareCurveData( xspan,time_sol(end,2:end));

% Set up fitype and options.

ft3 = 'pchipinterp';

% Fit model to data.

[fitresult3, gof3] = fit( xData, yData, ft3, 'Normalize', 'on' );

    %else
    %   tempinicond=sol(end,:);t_current=t_current+tday(end);
    %   time_sol=[time_sol;t_current/86400 tempinicond];
    %   save(name, '-append', 'time_sol');
    %end
end
clear tempinicond
clear sol
clear time_sol
end

% 7. Functions %%%%%%%%%%%%%%%%%%%%%%%%%%%%%%%%%%%%%%%%%%%%%%%%%%%%%%%%%%%%%%%%%%%%%%%%%

function u0 = inicond(x)
global fitresult3
u0 = fitresult3(x);
end

% PDE
function [c,f,s] = parab2(x,t,h,dhdx)
global K
c = 1; % Coefficient multiplying dEta/dt is 1
if -dhdx<0
    op=0;
elseif -dhdx==0
    op=0.5;
else
    op=1;
end
J=-dhdx*op;%J=S0;

```

```

f = -(4/7)*K*(J)^(7/4); % function f(I,f,K,S)
%f = K*(J)^(3/4); % function f(I,f,K,S)
s = 0; % No "s" term summing in the partial differential equation
end

% Boundary conditions

%general form: p(x,t,h)+q(x,t,h)*f(x,t,h,dh/dx)
function [pL,qL,pR,qR] = bcfun3(xL,uL,xR,uR,t)
%xL is the left boundary; xR is the right boundary
global S0 Eta0 L
pL = uL-345.72;qL = 0; %at the left boundary the sediment flux is zero
pR = uR-293.03;qR = 0; %at the right boundary the sediment flux is zero
end

```

11 Annex 3: Results processing code

```
clear all
close all

p1=load('simulation 5 years threshold = 01.mat');
p2=load('simulation 5 years threshold = 02.mat');
p3=load('simulation 5 years threshold = 03.mat');
p4=load('simulation 5 years threshold = 04.mat');
p5=load('simulation 5 years threshold = 05.mat');
p6=load('simulation 5 years threshold = 06.mat');
p7=load('simulation 5 years threshold = 07.mat');
p8=load('simulation 5 years threshold = 08.mat');
p9=load('simulation 5 years threshold = 09.mat');
p10=load('simulation 5 years threshold = 010.mat');
p11=load('simulation 5 years threshold = 011.mat');
p12=load('simulation 5 years threshold = 012.mat');
p13=load('simulation 5 years threshold = 013.mat');

years=5;%period of time of intrest
dt=1;% days interval
mesi=1:dt:years*365;
L=11726;dx=20;xspan=0:dx:L;
p1=p1.time_sol;p2=p2.time_sol;p3=p3.time_sol;p4=p4.time_sol;
p5=p5.time_sol;
p6=p6.time_sol;p7=p7.time_sol;p8=p8.time_sol;p9=p9.time_sol;
p10=p10.time_sol;p11=p11.time_sol;p12=p12.time_sol;p13=p13.time_sol;
p1=p1(mesi,2:end);p2=p2(mesi,2:end);p3=p3(mesi,2:end);p4=p4(mesi,2:end);
p5=p5(mesi,2:end);
p6=p6(mesi,2:end);p7=p7(mesi,2:end);p8=p8(mesi,2:end);p9=p9(mesi,2:end);
p10=p10(mesi,2:end);p11=p11(mesi,2:end);p12=p12(mesi,2:end);
p13=p13(mesi,2:end);

pmean=(p1+p2+p3+p4+p5+p6+p7+p8+p9+p10+p11+p12+p13)/13;
%desvest=std(p1,p2,p3,p4,p5,p6,p7,p8,p9,p10,p1,p12,p13);
figure (1)
plot(xspan,pmean)
legend

bmean=76.05;%[m] mean width of the reach
loi=500;%[m] length of interest before the dam, for the calculation of
the moved volume
abscisa2=6780;% [m] Dam's abscisa
abscisa1=abscisa2-loi;% [m] Starting abscisa before the dam
i1=find(abscisa1==xspan);% Index of abscisa 1
i2=find(abscisa2==xspan);% Index of abscisa 2
Vol(1,:)=zeros(1,length(i1:i2));% Initial change of volume
```

```

for i=2:length(pmean(:,1))
    Vol(i,:)=(pmean(i-1,i1:i2)-pmean(i,i1:i2))*bmean*dx;
    V(i)=sum(Vol(i,find(Vol(i,*)>0)));
    diff_y=(pmean(i-1,i1:i2)-pmean(i,i1:i2));
    diff_y(find(diff_y<0))=0;
    Vol2(i,:)=trapz(xspan(i1:i2),diff_y)*bmean;
    V2(i)=sum(Vol2(i,find(Vol2(i,*)>0)));
end

figure (2)
%plot(mesi,V)
%hold on
plot(mesi,V2)
title('Volume of sediments moved from upstream the dam ')
xlabel('time [days]')
ylabel('Volume [m^3]')

figure (3)
%plot(mesi,cumsum(V))
%hold on
plot(mesi,cumsum(V2))
title('Cumulated volume')
xlabel('Time [days]')
ylabel('Volume [m^3]')

Vf=cumsum(V2);Vf=Vf(end)
save('Cum_vol_5years_0.mat','Vf')

maxvol=0;
sum(V2(257:387))
maxvol=max(V2)
find(V2==maxvol)

% for i=1:365*5
%     figure (4)
%     plot(xspan,p4.time_sol(1,2:end))
%     xlim([6000 9000]);
%     hold on
%     plot(xspan,p4.time_sol(i,2:end))
%     hold on
% end

figure (5)
plot(xspan,pmean(1,:))
hold on
plot(xspan,pmean(end,:))
title('Final profile after 5 years')
xlabel('Abscisa [m]')
ylabel('Elevation [m]')

```

```

        legend('Initial profile','Final profile')

%Mesh plot
figure (7)
mesh(xspan(308:470),mesi/365,pmean(:,308:470))
xlabel('Abcisa [m]')
ylabel('Time [years]')
c=colorbar;
c.Label.String = 'Elevation [m.a.s.l.]';

pmean2=zeros(length(pmean));
for i=1:length(pmean)
pmean2(i,308:470)=pmean(i,308:470)-pmean(end,308:470);
end

%X - t plot
figure (8)
[X,Y]=meshgrid(xspan(308:470),mesi/365);
H=pcolor(X,Y,pmean2(:,308:470));
set(H,'edgecolor','none');c=colorbar;colormap jet;hold on;
c.Label.String = 'Difference in elevation [m]';
xlabel('Abcisa [m]');ylabel('Time [years]');

%at $x=6140 m$ at 530037.787 E 4954022.330 N and finishes at $x=9508 m$
% dam located at $x=6770 m$

```

References

- [1] *A San Salvatore test per abbattere la diga. I residenti sbarrano le strade.* 2022. URL: <https://www.liberta.it/news/cronaca/2022/04/13/a-san-salvatore-test-per-abbattere-la-diga-i-residenti-sbarrano-le-strade/>. Giornale Libertà.
- [2] S. Acharya. “Assesing the feasibility of San Salvatore dam removal on the Trebbia River: A study of river restoration and hydromorphological effects through numerical simulation”. PhD thesis. Politecnico di Torino, 2018.
- [3] A. Agogliati. *L’energia idroelettrica nel bacino Trebbia-Aveto.* 2008. URL: https://www.valdaveto.net/documento_814.html. Val d’Aveto official website.
- [4] Christophe Ancey. “Bedload transport: a walk between randomness and determinism. Part 1. The state of the art”. In: *Journal of Hydraulic Research* 58.1 (2020), pp. 1–17. DOI: 10.1080/00221686.2019.1702594. URL: <https://doi.org/10.1080/00221686.2019.1702594>.
- [5] ARPA. *Hydrological annual reports.* Tech. rep. Regional Agency for the Environmental Protection (ARPA) Emilia-Romagna, 2022.
- [6] Jones J. Belletti B. Garcia de Leaniz C. and et al. (2020). “More than one million barriers fragment Europe’s rivers”. In: (2020). DOI: <https://doi.org/10.1038/s41586-020-3005-2>.
- [7] J. J. Craig L. S. Greene S. L. Torgersen C. E. Collins M. J. Bellmore J. R. Duda and Vittum. “Status and trends of dam removal research in the United States”. In: (2017). DOI: <https://doi.org/10.1002/wat2.1164>.
- [8] C. Camporeale. “Hydro-informatics Lab 6: Dam filling”. River Engineering and Restoration - DM270. 2022.
- [9] C. Camporeale. “Section 3. Sediment Mechanics”. River Engineering and Restoration - DM270. 2022.
- [10] C. Camporeale. “Section 4. Morphodynamics. Part A”. River Engineering and Restoration - DM270. 2022.
- [11] A. Cantelli et al. “Numerical model linking bed and bank evolution of incisional channel created by dam removal”. In: *Water Resources Research* 43.7 (2007). DOI: <https://doi.org/10.1029/2006WR005621>. URL: <https://agupubs.onlinelibrary.wiley.com/doi/abs/10.1029/2006WR005621>.
- [12] *Daily discharge of Bobbio gauge station.* 2023. URL: <https://simc.arpae.it/dext3r/>. Dext3r webapp to download data from ARPA Emilia-Romagna.
- [13] “San Salvatore Dam: 100 years waiting to be removed (+ some considerations on dam removal in Italy)”. In: 2022.
- [14] S. Dey. *Fluvial Hydrodynamics: Hydrodynamic and Sediment Transport Phenomena.* GeoPlanet: Earth and Planetary Sciences. Springer, 2014.
- [15] Liuyong Ding et al. “Global Trends in Dam Removal and Related Research: A Systematic Review Based on Associated Datasets and Bibliometric Analysis”. In: *Chinese Geographical Science* (Oct. 2018). DOI: 10.1007/s11769-018-1009-8.
- [16] A. Porporato E. Daly. “Some self-similar solutions in river morphodynamics”. In: *Water REsources REsearch, Volume 41, Issue 12* (2005). DOI: <https://doi.org/10.1029/2005WR004488>.
- [17] A. E. East et al. “Geomorphic Evolution of a Gravel-Bed River Under Sediment-Starved Versus Sediment-Rich Conditions: River Response to the World’s Largest Dam Removal”. In: *Journal of Geophysical Research: Earth Surface* 123.12

- (2018), pp. 3338–3369. DOI: <https://doi.org/10.1029/2018JF004703>. eprint: <https://agupubs.onlinelibrary.wiley.com/doi/pdf/10.1029/2018JF004703>. URL: <https://agupubs.onlinelibrary.wiley.com/doi/abs/10.1029/2018JF004703>.
- [18] H. A. Einstein. *The Bed-Load Function for Sediment Transportation in Open Channel Flows*. Tech. rep. Soil conservation service (SCS), 1950.
- [19] ARPA Emilia-Romagna. “Hourly discharge data of Bobbio gauge station”. provided by email from: Arpae - Struttura Idro-Meteo-Clima, Servizio Idrografia e Idrologia Regionale e Distretto Po.
- [20] ARPA Emilia-Romagna. *Studio del bacino idrografico del fiume Trebbia per la gestione sostenibile delle risorse idriche*. Tech. rep. 2008.
- [21] F. Engelund and E. Hansen. “A Monograph on Sediment Transport in Alluvial Streams”. In: *Teknisk forlag* (1967). URL: <http://resolver.tudelft.nl/uuid:81101b08-04b5-4082-9121-861949c336c9>.
- [22] Mouchlianitis F.A. “Dam removal progress 2021”. In: (2022). URL: https://damremoval.eu/wp-content/uploads/2022/05/0.-REPORT_Dam-Removal-Progress-2021-WEB-SPREADS.pdf.
- [23] *Frequently asked questions about river restoration*. 2023. URL: <https://www.americanrivers.org/frequently-asked-questions-about-river-restoration/#:~:text=Rivers%20are%20very%20dynamic%20and,relatively%20rapidly%20after%20dam%20removal..> American rivers ORG.
- [24] Parker G. *1D Sediment Transport Morphodynamics with Applications to Rivers and Turbidity Currents*. University of Illinois, 2004.
- [25] WALTER H. GRAF and ERTAN R. ACAROGLU. “SEDIMENT TRANSPORT IN CONVEYANCE SYSTEMS (PART 1) / A PHYSICAL MODEL FOR SEDIMENT TRANSPORT IN CONVEYANCE SYSTEMS”. In: *International Association of Scientific Hydrology. Bulletin* 13.2 (1968), pp. 20–39. DOI: 10.1080/02626666809493581. URL: <https://doi.org/10.1080/02626666809493581>.
- [26] John R. Gray and Francisco J. M. Simões. “Estimating Sediment Discharge”. In: *Sedimentation Engineering*. Chap. Appendix D, pp. 1067–1088. DOI: 10.1061/9780784408148.apd. eprint: <https://ascelibrary.org/doi/pdf/10.1061/9780784408148.apd>. URL: <https://ascelibrary.org/doi/abs/10.1061/9780784408148.apd>.
- [27] E. Rondoni I. Bisetti M. Cazzoli and C. Spotorno. *Parco Fluviale del Trebbia*. 2012. URL: <https://www.parchidelducato.it/parco.trebbia/pagina.php?id=44>. Assessorato Ambiente e Riqualificazione Urbana della Regione Emilia-Romagna.
- [28] D. Woodward K. Kent and C. Hoefft. “Hydrology National Engineering Handbook”. In: Natural Resources Conservation Service, 2010. Chap. Chapter 15 “Time of concentration”.
- [29] T. Tormos K. van Looy and Y. Souchon. “Disentangling dam impacts in river networks”. In: (2014). URL: <https://hal.science/hal-00916423/file/ly2014-pub00039414.pdf>.
- [30] M. Fazle Karim and John F. Kennedy. “Menu of Coupled Velocity and Sediment-Discharge Relations for Rivers”. In: *Journal of Hydraulic Engineering* 116.8 (1990), pp. 978–996. DOI: 10.1061/(ASCE)0733-9429(1990)116:8(978). URL: <https://ascelibrary.org/doi/abs/10.1061/%28ASCE%290733-9429%281990%29116%3A8%28978%29>.

- [31] Bimlesh Kumar. “Neural network prediction of bed material load transport”. In: *Hydrological Sciences Journal* 57.5 (2012), pp. 956–966. DOI: 10.1080/02626667.2012.687108. URL: <https://doi.org/10.1080/02626667.2012.687108>.
- [32] Brent J. Lewis, E. Nihan Onder, and Andrew A. Prudil. “Chapter 5 - Partial differential equations”. In: *Advanced Mathematics for Engineering Students*. Ed. by Brent J. Lewis, E. Nihan Onder, and Andrew A. Prudil. Butterworth-Heinemann, 2022, pp. 131–164. ISBN: 978-0-12-823681-9. DOI: <https://doi.org/10.1016/B978-0-12-823681-9.00013-7>. URL: <https://www.sciencedirect.com/science/article/pii/B9780128236819000137>.
- [33] Bohlen C. Lewis L and Wilson S. “Dams, dam removal, and river restoration: a hedonic property value analysis”. In: (2008). DOI: [doi:10.1111/j.1465-7287.2008.00100.x](https://doi.org/10.1111/j.1465-7287.2008.00100.x).
- [34] E. Di Stefano R. Giulianelli P. Nardone M. Ciotti A. Ciuffetti and P. Raspadori. *Proposte e ricerche - Economia e società nella storia dell’Italia centrale*. eum edizioni università di macerata, 2016.
- [35] M. Marini. *Val Trebbia, cittadini e ambientalisti contro la diga*. 2013. URL: https://www.ilcambiamento.it/articoli/val_trebbia_cittadini_ambientalisti_contro_diga. Il cambiamento.
- [36] Autorità di bacino del fiume Po. *General lines of hydraulic and hydrogeological structure in the Trebbia basin*. 2009. URL: <https://www.adbpo.it/PAI/3%20-%20Linee%20generali%20di%20assetto%20idraulico%20e%20idrogeologico/3.4%20-%20Elaborato%20Emilia-Romagna/Trebbia.pdf>. Autorità di bacino del fiume Po.
- [37] Autorità di bacino del fiume Po. *Progetto di Piano per la valutazione e la gestione del rischio di alluvioni*. Tech. rep. Primo Piano di gestione del rischio di alluvioni (PGRA 2015-2021) Sezione B (D.Lgs. n. 49/10 art 7, comma 3 lettera b) Relazione Regione Emilia-Romagna, 2015.
- [38] *RIMOZIONE DI SBARRAMENTI LUNGO I CORSI D’ACQUA: ITALIA FANALINO DI CODA D’EUROPA*. 2022. URL: <https://www.cirf.org/rimozione-di-sbarramenti-lungo-i-corsi-dacqua-italia-fanalino-di-coda-deuropa/>. Centro Italiano per la Riqualificazione fluviale.
- [39] F. Tauro S. Grimaldi A. Petroselli and M. Porfiri. “Time of concentration: a paradox in modern hydrology”. In: *Hydrological Sciences Journal* 57.2 (2012), pp. 217–228. DOI: 10.1080/02626667.2011.644244. eprint: <https://doi.org/10.1080/02626667.2011.644244>. URL: <https://doi.org/10.1080/02626667.2011.644244>.
- [40] M. Favalli A. Battistini S. Tarquini I. Isola and G. Dotta. *A digital elevation model of Italy with a 10 meters cell size (Version 1.1)*. 2023. URL: <https://doi.org/10.13127/tinitaly/1.1>. Istituto Nazionale di Geofisica e Vulcanologia (INGV).
- [41] N. Sala and R. van Treeck. “Dam removal progress 2020”. In: (2021). URL: <https://damremoval.eu/wp-content/uploads/2021/06/Dam-Removal-Progress-2020-Spreads.pdf>.
- [42] Deepti Shakya et al. “Predicting Total Sediment Load Transport in Rivers Using Regression Techniques, Extreme Learning and Deep Learning Models”. In: *Artif. Intell. Rev.* 56.9 (2023), pp. 10067–10098. ISSN: 0269-2821. DOI:

- 10.1007/s10462-023-10422-6. URL:
<https://doi.org/10.1007/s10462-023-10422-6>.
- [43] *Shapefile of rivers tributants to the Po*. 2021. URL: https://webgis.adbpo.it/geoserver/ows?service=WFS&version=1.0.0&request=GetFeature&typename=geonode%3APdgPo2021_Fiumi&outputFormat=SHAPE-ZIP&srs=EPSG%3A3035&format_options=charset%3AUTF-8. Autorità di bacino del fiume Po.
- [44] L. Toso. “Estimating sediment transport in the Mogtedo watershed, Burkina Faso”. PhD thesis. Politecnico di Torino, 2018.
- [45] P. Vezza. “European directives on freshwater river management”. *River Engineering and Restoration - DM270*. 2022.
- [46] Andrew C. Wilcox, Jim E. O’Connor, and Major Jon J. “Rapid reservoir erosion, hyperconcentrated flow, and downstream deposition triggered by breaching of 38 m tall Condit Dam, White Salmon River, Washington”. In: *Journal of Geophysical Research: Earth Surface* 119.6 (2014), pp. 1376–1394. DOI: <https://doi.org/10.1002/2013JF003073>. URL: <https://agupubs.onlinelibrary.wiley.com/doi/abs/10.1002/2013JF003073>.
- [47] Chih Ted Yang. “Unit Stream Power and Sediment Transport”. In: *Journal of the Hydraulics Division* 98.10 (1972), pp. 1805–1826. DOI: 10.1061/JYCEAJ.0003439. URL: <https://ascelibrary.org/doi/abs/10.1061/JYCEAJ.0003439>.
- [48] Shu-Qing Yang. “Prediction of total bed material discharge”. In: *Journal of Hydraulic Research* 43.1 (2005), pp. 12–22. DOI: 10.1080/00221680509500107. URL: <https://doi.org/10.1080/00221680509500107>.